Environmental Drivers of Arctic Low-Level Clouds: Analysis of the Regional and Seasonal Dependencies Using Space-Based Lidar and Radar

Aymeric Dziduch, Guillaume Mioche, Quentin Coopman, Clément Bazantay, Julien Delanoë, Olivier Jourdan

https://doi.org/10.5194/egusphere-2025-2698
Preprint. Discussion started: 3 July 2025

Environmental Drivers of Arctic Low-Level Clouds: Analysis of the Regional and Seasonal Dependencies Using Space-Based Lidar and Radar

Aymeric Dziduch[1], Guillaume Mioche[1*], Quentin Coopman[2], Clément Bazantay[1], Julien Delanoë[3] and Olivier Jourdan[1*]

[1]Université Clermont Auvergne, OPGC, Laboratoire de Météorologie Physique, 63000 Clermont-Ferrand, France
[2]Univ. Lille, CNRS, UMR 8518 - LOA - Laboratoire d'Optique Atmosphérique, F-59000 Lille, France
[3]LATMOS/IPSL, UVSQ Université Paris-Saclay, Sorbonne Université, CNRS, Guyancourt, France

Correspondence. Olivier Jourdan (Olivier.Jourdan@uca.fr) and Guillaume Mioche (Guillaume.Mioche@uca.fr)

Abstract. Low-level clouds play a crucial role in the Arctic surface energy budget and hydrological cycle. However, their representation in climate models remains challenging due to limited observations and complex interactions between local processes and large-scale environmental conditions. This study analyzes eight years of active remote sensing observations from CALIPSO and CloudSat to investigate the regional and seasonal distribution of four types of low-level clouds: warm liquid, ice-only, mixed-phase clouds (MPCs), and unglaciated supercooled liquid clouds (USLCs). Our results show that 51% of low-level clouds are located below 3 km. A reassessment of cloud-type frequencies reveals that MPCs occur 17% of the time, ice-only clouds 20%, and USLCs 12%. Notably, this work provides the first satellite-based assessment of USLCs over the Arctic, showing that their occurrence can reach up to 25% in oceanic regions during transition seasons. The Svalbard region and Bering Seas emerge as the cloudiest areas, where liquid-containing clouds are prevalent, while ice clouds dominate over Alaska and Siberia. Using multiple linear regression, we quantify the influence of key environmental drivers on cloud-phase occurrence. Surface temperature, lower tropospheric stability, mid-tropospheric humidity, and marine cold air outbreaks (MCAOs) are identified as dominant factors. MPCs are particularly linked to dynamic conditions such as MCAOs, especially over oceanic regions and during transition seasons, whereas USLCs are more associated with stable and drier mid-tropospheric environments. The results highlight the impact of air mass intrusions on the regional distribution of the cloud phase partitioning, offering guidance for improving their representation in climate models.

Keywords. Arctic, low-level clouds, thermodynamic phase, occurrence

1 Introduction

The Arctic region is sensitive to climate change and has warmed almost four times faster than the rest of the globe, a phenomenon known as Arctic Amplification (Rantanen et al., 2022). The Arctic is a cloudy region with an annual mean cloud cover higher than 70% (Matus and L'Ecuyer, 2017; Boccolari and Parmiggiani, 2018; Wang et al., 2021; Lelli et al., 2023). Clouds play an essential role in the energy and water balance of the Arctic climate

https://doi.org/10.5194/egusphere-2025-2698
Preprint. Discussion started: 3 July 2025

system. In particular, they modulate energy exchanges at the surface (Sedlar et al., 2012; Yan et al., 2020). Estimates of the net cloud radiative effect (CRE) at the surface based on CALIPSO/CloudSat observations suggest annual averages of about 10 to 15 W/m² over the Northern Arctic (Kay and L'Ecuyer, 2013; Matus and L'Ecuyer, 2017). These values are significantly higher than those previously estimated using passive satellite remote sensing observations (Schweiger and Key, 1992; Wang and Key, 2005; Dong et al., 2010). At the surface, the CRE is characterized by a pronounced seasonal variability, with a warming effect from mid-August to April or May and a cooling influence during the rest of the year. This seasonal pattern results from the amount of solar radiation reaching the lower layers of the troposphere and the surface but also from the seasonal variability of the cloud cover, the cloud thermodynamic phase, and the lower atmospheric stability (Kay and L'Ecuyer, 2013; Kay et al., 2016; Ebell et al., 2020; Philipp et al., 2020).

Statistical analysis of ground-based observations highlights strong regional disparities and seasonality in net CRE at the surface. For instance, the annual average of CRE varies from 33 W/m² at the Summit station in Greenland (Miller et al., 2015) to 11 W/m² at Ny-Ålesund in Svalbard (Ebell et al., 2020) and 4.5 W/m² over Barrow, Alaska (Dong et al., 2010). More recently, studies based on satellite observations have also confirmed the existence of pronounced inter-regional variations (Lelli et al., 2023; Cesana et al., 2024). Geographical variations are mostly driven by changes in the shortwave radiation (SW) linked to the variability of the solar zenith angle and to the surface conditions (Intrieri et al., 2002; Screen and Simmonds, 2010; Kay and L'Ecuyer, 2013). However, the CRE in the longwave (LW) is also influenced by regional changes in temperature, humidity (Cox et al., 2012, 2015), and cloud properties (Shupe and Intrieri, 2004; Ebell et al., 2020). In particular, Shupe and Intrieri (2004) showed that the LW CRE increases almost linearly with cloud cover (0.65 W/m² per % of cloud cover) and cloud temperature (1 W/m² per °C), while Ebell et al. (2020) found an exponential dependence with the liquid water path below values of 40 g.m^{-2}.

Airborne, ground-based, and satellite observations suggest that low-level clouds are common in most regions of the Arctic (De Boer et al., 2009; Wendisch et al., 2019; Philipp et al., 2020; Taylor and Monroe, 2023; Jiang et al., 2024). In particular, below 2-3 km, mixed-phase clouds (MPCs) and, more generally, liquid clouds occur frequently throughout the year (Cesana et al., 2012; Mioche et al., 2015; McIlhattan et al., 2017; Gierens et al., 2020). These clouds exert a strong influence on the surface energy budget with an annual warming effect (Raschke et al., 2016; Li et al., 2023). Few studies have been conducted to specifically understand and quantify regional and seasonal variations in the radiative effect of low clouds (Yan et al., 2020; Cesana et al., 2024). The CRE evolves strongly over time and shows pronounced variability, especially between the open ocean, sea ice-covered, and continental regions (Miller et al., 2015; Ebell et al., 2020). Moreover, Cesana et al. (2012) showed that climate models struggle to reproduce the seasonal variations in the radiative effect of low-level clouds due to an underestimation of the amount of liquid-containing clouds (Kay et al., 2016). More generally, the spatial inhomogeneities and temporal evolution of the low-level Arctic cloud properties are particularly difficult to model (Inoue et al., 2006; Wyser et al., 2008; Sedlar et al., 2012; Taylor et al., 2019) and pose a multi-decadal challenge to understanding their impacts (Curry et al., 1996; Tjernström et al., 2008; Vavrus et al., 2009; Li et al., 2023). Observational constraints on the persistence of low-level clouds and their microphysical properties (liquid and ice

https://doi.org/10.5194/egusphere-2025-2698
Preprint. Discussion started: 3 July 2025

water content, effective dimensions of hydrometeors, cloud thickness) are needed to improve the calculation of their radiative effect in the Arctic (Curry and Ebert, 1992; Sun and Shine, 1994; Shupe and Intrieri, 2004; Morrison et al., 2012).

First, it seems important to accurately assess the type and phase of low-level clouds over different regions of the Arctic. This is a prerequisite for estimating their microphysical properties and, ultimately, their radiative effects. In this respect, Kay et al. (2016) highlight the need to investigate not only the cloud cover but also the cloud phase distribution. One objective of our study is to investigate the geographical and seasonal distribution of low-level clouds and to provide statistically robust estimates of the regional frequency of occurrence of different cloud types.

Arctic low-level cloud properties are influenced by large-scale environmental conditions (Morrison et al., 2012; Li et al., 2020a, b; Griesche et al., 2021). In the context of significant changes in this region of the globe, low-level cloud fractions and properties may be affected by changes in surface type and meteorological conditions (Kay and Gettelman, 2009; Eastman and Warren, 2010; Liu and Schweiger, 2017; Morrison et al., 2019; Liu and Schweiger, 2024). For example, Cesana et al. (2024) observed a significant variation in cloud radiative properties and cloud fraction during the transition from ice pack to open ocean. Lower-tropospheric stability also influences low-level cloud occurrence, but the link between these properties is still poorly represented in models (Taylor & Monroe, 2023). Moser et al. (2023) and Mioche et al. (2017) have demonstrated a significant change in the in situ microphysical and macrophysical MPCs properties in the Svalbard region in relation to the origin of the air mass. Indeed, heat and moisture advection, often associated with phenomena such as warm air intrusions (WAI) or cold air outbreaks (CAO) from higher or lower latitudes, can induce rapid changes in local weather conditions and directly affect the formation and structure of low-level clouds (Lackner et al., 2023). The large-scale transport of aerosol particles can also modify the microphysical properties and the thermodynamic phase of low-level clouds (Bossioli et al., 2021; Schmale et al., 2021; Raut et al., 2022). These studies highlight the need to improve our understanding of how environmental conditions influence low-level cloud properties. The second objective of our study is to identify a set of key thermodynamic parameters that control or affect the regional distribution of the cloud phase.

To this end, we rely on the synergy of CALIPSO lidar and CLOUDSAT radar satellite measurements (DARDAR-MASK products, Delanoë and Hogan, 2008, 2010; Ceccaldi et al., 2013) to analyze cloudy scenes over different arctic regions. DARDAR products, combined with the DARDAR-SOCP classification algorithm, are used to determine the occurrence of the thermodynamic phase of low-level clouds. Section 2 describes the dataset, the DARDAR-SOCP classification algorithm, and the statistical analyses used to characterize cloud-type occurrences. The uncertainties and limitations associated with this methodology are also discussed. Section 3 presents the results on the spatial distribution and temporal variations of cloud-type occurrences. Multiple linear regressions (MLR) are also implemented to quantify the influence of key environmental parameters on cloud

https://doi.org/10.5194/egusphere-2025-2698
Preprint. Discussion started: 3 July 2025

occurrences. Section 4 offers a discussion of the results in relation to previous studies, while Section 5 provides the overall conclusion of the study.

2 Methods and Data

2.1 DARDAR retrieval products

In this study, we analyze the variability in the frequency of occurrence of several low-level cloud types from 2007 to 2016 in the Arctic region, defined here as the area between 60°N and 82°N latitude. While there is no universally fixed boundary, this definition follows conventions commonly used in recent studies (e.g., Eastman and Warren, 2009; Cesana et al., 2012, 2024; Mioche et al., 2015), and allows inclusion of key transitional zones relevant to cloud processes. Cloud-type occurrences are derived from DARDAR-MASKv2.23 products generated from the lidar/radar instrumental synergy (Delanoë and Hogan, 2010). Observations from the CALIOP lidar onboard the CALIPSO satellite (McGill et al., 2007; Winker et al., 2007) and the CloudSat cloud profiling radar (CPR) (Stephens et al., 2002) are merged on the same resolution grid. The CALIPSO and CLOUDSAT satellites are part of the A-Train constellation, which has an orbital period of 98.5 minutes. This allows the constellation to pass over the Arctic region up to 14 times per day.

The CALIOP lidar operates at two wavelengths (532 and 1064 nm). Only the 532 nm wavelength is used for the DARDAR products because it is highly effective in measuring small cloud particles. The lidar signal is sensitive to optical extinction, which is directly influenced by the concentration of cloud particles and their shape. It can be rapidly attenuated in clouds with optical depth higher than 3 to 5 depending on their microphysical composition (Chepfer et al., 2014). The Cloud Profiling Radar (CPR) operates at a frequency of 94 GHz (W-band). The radar signal is more sensitive to the size of hydrometeors and therefore more likely to detect large cloud particles (ice crystals) present in clouds and precipitation. CPR has an initial vertical resolution of 500 m, which is then interpolated to the same resolution as the CALIOP lidar (60 m). The CALIOP "Level-1B 532 nm lidar backscatter coefficient" profiles (Winker et al., 2007) are merged with the CPR "2B-GEOPROF radar reflectivity" (Marchand et al., 2008) profiles on the same resolution grid. The horizontal resolution of the products is defined by the CPR radar with 1.7 km along the track and 1.4 km across the track. Vertical profiles of cloud layer properties can be obtained by combining the two instruments, overcoming the limitations of each.

Originally developed by Delanoë et Hogan (2008, 2010), a second version of DARDAR-mask products was implemented by Ceccaldi et al. (2013), introducing new cloud classes based on the type of hydrometeors detected. The satellite product is derived from an algorithm that analyzes lidar signals (attenuated backscattering) and radar signals (reflectivity) to classify each pixel of the atmosphere and assign it a cloud class (algorithm diagram in Ceccaldi et al. 2013, Fig. 5). In DARDAR-MASK products, each atmospheric pixel (60 m vertically and 1.7 km along the track) is assigned a specific class ranging from -2 to 15. Class determination is based on thresholds for attenuated backscattering and reflectivity combined with thermodynamic data (temperature) and layer thickness. Warm liquid water is identified by strong lidar attenuation ($\beta_{532nm} \geq 2.\ 10^{-5} m^{-1} sr^{-1}$) and positive temperature ($T > 0°C$). Supercooled liquid water is determined by strong lidar attenuation, negative temperature ($-40°C < T < 0°C$),

https://doi.org/10.5194/egusphere-2025-2698
Preprint. Discussion started: 3 July 2025

and layer thickness below 360 m. The mixed phase of supercooled liquid water droplets and ice crystals is distinguished from supercooled water droplets alone by the presence of radar reflectivity. In all other cases, the algorithm classifies the cloud phase as ice. These 18 DARDAR-MASK classes (**Figure S1**, in Supporting Information) correspond to different atmospheric features: surface detection problems or errors (classes -2, -1, and 15), cloud-free (class 0), aerosols (class 6), and stratospheric textures (class 8). The remaining classes represent the type of cloud layers used in the cloud classification algorithm.

2.2 Cloud classification program DARDAR-SOCP

A first classification program was implemented by Mioche et al. (2015) to study mixed-phase clouds in the Arctic region. Bazantay et al. (2024) introduced a new cloud classification program for the Southern Ocean (DARDAR-SOCP, for Southern Ocean Cloud Phase). In this paper, we use the same program as in Bazantay et al. (2024), adapting it to study the Arctic region. A more detailed description of the DARDAR-SOCP cloud classification program can be found in Bazantay et al. (2024).

The DARDAR-SOCP program analyzes DARDAR-MASKv2.23 classes for each atmospheric column (500 to 3000 m) to determine the different cloud types observed within the column. A cloud is defined by at least 3 vertically adjacent cloudy pixels (or 180 meters). This is consistent with in situ observations on the structure and thickness of low-level clouds in the Arctic (Achtert et al., 2020; Järvinen et al., 2023; Zanatta et al., 2023). The horizontal resolution of the cloud is defined by the size of the measurement pixels (i.e., 1.7 km). A column can contain two or more layers of clouds only if they are separated from each other by three non-cloudy adjacent pixels. The algorithm then determines the cloud type based on the classes determined by DARDAR. The DARDAR version 2 classes and the representation of clouds in DARDAR-SOCP are shown in **Figure S1** in Supporting Information. Warm clouds are composed exclusively of pixels containing hydrometeors in the liquid phase (classes 5, 7, 11, 12, 13, and 14) at a positive temperature. Cold clouds are composed of three types: Unglaciated Supercooled Liquid Clouds (USLCs) are defined exclusively by supercooled water droplet pixels (class 3). Ice clouds consist entirely of ice crystal pixels (classes 1, 2, 9, and 10) and d Mixed-Phase Clouds (MPCs), which are characterized by a mixture of pixels in different phases.

Cloud occurrences (OC_n) retrieved for each cloud type n (total, cold, warm, cold, ice, USLCs, or MPCs) based on the cloud classification: OC_n is the ratio of the number of cloud observations (N_n) to the number of satellite footprints ($N_{footprint}$). This ratio is expressed as a percentage using equation (1):

$$OC_n = \frac{N_n}{N_{footprint}} \times 100 \quad (1)$$

Each granule is processed by DARDAR-SOCP if it contains footprints between 60°N and 82°N. For each footprint, the program counts the number of cloudy pixels of a given cloud type by analyzing the column pixel by pixel. These counts are stored in boxes of 2° latitude by 2° longitude before the cloud type is retrieved. In this study, low-level clouds (between 500 and 3000 m) are analyzed over 8 years, from 2007 to 2010 and from 2013 to 2016. The years 2011 and 2012 are excluded due to a battery anomaly on the CloudSat satellite, which caused data loss (see Appendix A for more details). Before 2010, both daytime and nighttime observations were used, while after 2012, only daytime observations are considered due to the same battery-related issues.

https://doi.org/10.5194/egusphere-2025-2698
Preprint. Discussion started: 3 July 2025

2.3 Limitations and uncertainties

DARDAR cloud-type classification and occurrence are subject to 3 types of uncertainty: instrumental/measurement, phase detection, and statistical. Errors associated with DARDAR-MASK products are mainly due to the limitations of the instruments and the measurement techniques. Observations at low altitudes (between 0 and 500 m) are contaminated by ground echoes. CloudSat CPR's pulse generates a surface clutter echo that tends to partially mask clouds near the surface (Marchand et al., 2008), leading to measurement bias and overestimation of low-level clouds. As shown in Liu (2022), lidar alone underestimates the occurrence by 25% below 600 m and 9% between 600 m and 1 km compared to surface observations. Mioche et al. (2015) have quantified the uncertainties in the occurrence estimation of low-level clouds at altitudes between 500 and 1000 m, finding a discrepancy of nearly 10% between DARDAR and ground-based observations. In addition, Mioche and Jourdan (2018) highlighted pixel classification issues between the DARDAR cloud mask and phase assessment using in situ data. The comparison showed 80% agreement between the two datasets for the liquid phase and 50% agreement for the ice phase. The main sources of disagreement came from near-surface pixels, both radar echo contamination and lidar attenuation. This study shows that the uncertainty of cloud occurrence between 500 m and 2 km is greater than 20%. The CALIOP lidar is completely attenuated by clouds with optical thickness greater than 3 (Winker et al., 2007). As a result, the lidar tends to be very sensitive to the upper phase of the cloud (Cesana et al., 2016). This has a direct impact on the DARDAR algorithm, as in the absence of information from the lidar, the cloud phase is only diagnosed based on the radar and could therefore underestimate the occurrence of USLCs. Bazantay et al. (2024) estimated that cloud detection was made from radar alone between 4 and 6% of the time.

In DARDAR-SOCP, cloud-type occurrences are estimated based on the assumption that a cloud necessarily contains at least 3 consecutive cloudy pixels. Given that mixed-phase clouds are generally composed of several single-phase layers (Mioche et al., 2017; Moser et al., 2023), this choice introduces a potential accumulation of errors in the detection of mixed-phase clouds. Bazantay et al. (2024) have shown that the occurrence of MPCs may be overestimated compared to ice clouds and warm clouds. The uncertainties associated with each type of cloud were estimated to be 15% for ice clouds, 20% for warm clouds, and 10% for MPCs. These uncertainties can increase rapidly for MPCs (close to 80% uncertainty) if several consecutive DARDAR pixels are classified as "mixed" instead of "liquid" or "ice" pixels.

2.4 Definition of environmental factors

Thermodynamic data are used to analyze the impact of environmental conditions on cloud presence and type. DARDAR-SOCP retrieves thermodynamic variables from ECMWF analyses, which are integrated into DARDAR-MASK files as part of the ECMWF-AUX collocated products (Delanoë et al., 2011; Hersbach et al., 2020). ECMWF-AUX is an intermediate product where the thermodynamic properties of the ECMWF model are interpolated between each CPR radar profile. The interpolation uses meteorological data from ECMWF 3-hour forecasts on a 0.5°x0.5° grid (Cronk et Partain, 2017). For each footprint where a cloud is detected, surface air temperature and pressure, specific humidity, and geopotential heights at 700 and 850 hPa are extracted. Additionally, Lower-Tropospheric Stability ($LTS = \theta_{700hPa} - \theta_{1000hPa}$, Wood and Bretherton, 2006) and Marine

https://doi.org/10.5194/egusphere-2025-2698
Preprint. Discussion started: 3 July 2025

Cold Air Outbreak ($MCAO = \theta_{800hPa} - \theta_{skin}$, Fletcher et al., 2016) are retrieved and averaged over a week and on a 2° × 2° grid cell.

Sea ice concentration (SIC) data are obtained using the AMSR-E (Advanced Microwave Scanning Radiometer for EOS) instrument onboard the AQUA satellite from 2002 to 2011, and subsequently the AMSR2 (Advanced Microwave Scanning Radiometer 2) instrument onboard the GCOM-W1 (Global Change Observation Mission-Water 1) satellite from 2012 to the present (Shibata et al., 2003). These two passive microwave radiometers measure brightness temperatures in different channels (18, 23, 37, and 89 GHz). The spatial resolution of the measurements varies depending on the channel; e.g., 5.4 km for the 89.0 GHz channel. The satellite data are processed using the ARTIST Sea Ice (ASI) algorithm (Spreen et al., 2008; Du et al., 2017). This algorithm has been validated by comparisons with other processing algorithms and in situ sea ice concentration data (Wiebe et al., 2009). The commonly accepted error for a sea ice concentration of 100% is 5.7% (Spreen et al., 2008). The data used in this study are level 2 with a spatial resolution of 6.25 km.

We use CALIPSO measurements ("01kmCLay.v4.20" product, Young and Vaughan, 2009) to access the aerosol optical depth (AOD) based on the extinction and backscattering profiles of particles. Aerosol profiles are generated with a vertical resolution of 60 m in the troposphere and a horizontal resolution of 5 km with an altitude range between 30 km and -0.5 km. The lidar products provide extinction coefficients for the two wavelengths of the instrument (532 and 1064 nm). In this study, the aerosol optical depth (AOD) is calculated from the extinction coefficient at 532 nm for each granule associated with the DARDAR data. A cloud/aerosol discrimination score ("CAD score") is used to distinguish cloudy pixels from pixels with aerosol present (Liu et al., 2009, 2019). More than 90% of all detected layers have a confidence level greater than 70% (|CAD score| > 70). The uncertainty associated with the determination of the optical thickness (aerosol extinction) comes from the associated lidar S ratio. The uncertainty is about 50% for an AOD = 0.5, and the associated uncertainty increases for higher AOD values. To investigate the relationships between cloud occurrence, sea ice concentration, aerosol optical depth, and meteorological parameters, the data are processed in a similar way to the DARDAR data. The data are adjusted to the study area, between 60° and 82° N, and averaged over grid cells of 2° latitude and 2° longitude.

3. Results

3.1 Geographical variability of low-level cloud occurrences

This section examines the occurrence of clouds (OC) derived from DARDAR-MASK products processed with DARDAR-SOCP over different regions of the Arctic. Over the entire atmospheric column (between 0.5 and 12 km), clouds are present 69% of the time in the Arctic (not shown here). The stereographic projections shown in **Figures 1a-f** highlight the heterogeneous spatial/geographical distribution of cloud cover over the Arctic. Over the entire Arctic region, the median annual occurrence of low-level clouds ($OC_{all\text{-}ll}$), between 0.5 and 3 km, is 51% (**Fig. 1a**). The vast majority of these clouds ($OC_{cold\text{-}ll}$ = 48.8% out of 50.9%) evolve in an environment where the

https://doi.org/10.5194/egusphere-2025-2698
Preprint. Discussion started: 3 July 2025

temperature is below 0°C. This occurrence decreases at lower latitudes, especially over oceanic regions. **Figures 1a** and **1f** indicate that the total cloud and MPC occurrences vary significantly between oceanic and continental regions. **Figure 1c** shows the occurrence of warm liquid clouds (OC_{warm}). Warm clouds are present less than 3% of the time. OC_{warm} is more pronounced in low-latitude oceanic regions such as over the North Atlantic, where these clouds are observed up to 15% of the time. The averaged distribution of fully glaciated cloud occurrences (OC_{ice}) shows strong geographical contrasts. OC_{ice} averages close to 21% over the Arctic but reaches 30-35% over continental and mountainous regions (**Fig. 1d**). Clouds composed entirely of supercooled water droplets (USCLs) are less common than ice clouds (**Fig. 1e**). They occur no more than 12% of the time (OC_{USLCs}). Mixed-phase clouds (**Fig. 1f**), characterized by a mixture of water droplets and ice crystals, are observed on average 17% of the time over the Arctic.

The spatial analysis of the occurrence of different types of low-level clouds and the use of Arctic weather reanalysis allow us to propose a regionalization of the study area into several regions. The continental zones of Russia, Europe, Canada, and Alaska were segmented using OC_{ice} and OC_{USLCs}. Alaska and Western Canada are more covered by ice clouds (OC_{ice} > 25%) than eastern Canada. The geographical pattern of their occurrence (OC_{MPCs}) is similar to that of the USLCs and the total low-level clouds. **Figure 2a** shows the regionalization of the study area. This regionalization was done to highlight the heterogeneities of cloud occurrence in the Arctic region described above. Region 1A was defined using the stereographic map of warm clouds; this is the area with the highest occurrence of warm clouds. Region 2F is defined between 74°N and 82°N to separate the ocean/sea ice zone from the continental-influenced region 1G. In addition, some regions (1-2C and 1-2B) have been merged to improve statistical representativeness. For the Greenland region (region 1-2B), the zone remains complex to analyze because of the high relief (weaker column analyzed and therefore less representative).

The highest values of $OC_{all\text{-}ll}$ are observed over oceanic regions such as the northeastern Atlantic region and the Svalbard region (referred to as zones 1A and 2A). Over the maritime sector covering the Greenland, Barents, and Norwegian Seas, low-level clouds are present more than 80% of the time (**Fig. 1a**). In contrast, some continental regions like Northern Russia (1G), Canada (1D), or Alaska (1E) have lower $OC_{all\text{-}ll}$ values of about 60%. Analysis of the cloud cover over Greenland is complicated by the orography of the region, leading to a significant bias near the surface due to radar clutter. Weather systems, such as high-pressure systems (Northern Russia–1G, **Fig. 1a**), have a direct influence on cloudiness in certain areas with a weak presence of low-level clouds ($OC_{all\text{-}ll}$ < 30%). In contrast, the Atlantic Ocean is a very cloudy area, with $OC_{all\text{-}ll}$ over 70% of the time, mostly influenced by the Gulf Stream and low-pressure systems. Moreover, in continental areas, $OC_{all\text{-}ll}$ is lower to the east of mountainous axes. This could be explained by the Foehn effect, which causes air masses to dry out (Shestakova et al., 2022). OC_{USLCs} are inhomogeneously distributed over the Arctic with a significant occurrence in the Svalbard region (2A), parts of Western Europe (1H), and Canada (1D) (between 15 and 25%, respectively, **Fig. 1e**). In contrast, continental regions such as Alaska (1E) and Russia (1G) show very low occurrence (< 10-15%) of this type of cloud. In particular, regional differences between continental and oceanic regions are well-defined, especially for regions between 60°W and 60°E. OC_{ice} follows a different pattern than other types of clouds. They are more present (> 30%) over continental areas and high latitudes such as Alaska (1E), Russia (1G), and the Eastern Arctic (2F). Mountainous/continental regions are associated with colder temperatures than oceanic

https://doi.org/10.5194/egusphere-2025-2698
Preprint. Discussion started: 3 July 2025

regions (**Fig. 1d**). OC_{MPCs} are highest in the North Atlantic sector (1A) and around the Svalbard archipelago (2A), with values exceeding 35% on average. In contrast, it is less than 15% over the continental plains of Canada (1D) and Siberia (1G). A more efficient vertical transport of water vapor then favors the initiation and maintenance of the liquid phase in clouds (Boisvert and Stroeve, 2015). Over the Bering Strait (1F), the frequency of occurrence of MPCs is 25% (**Fig. 1f**). This shows the influence of oceanic regions on coastal zones. In the Western Arctic (Alaska–1E), the coastal zone has a higher presence of mixed-phase clouds (about 20%). In contrast, the continental zone shows a lower occurrence, around 10%. A statistical analysis of total cloud occurrences is discussed in **Figure S2** in Supporting Information.

https://doi.org/10.5194/egusphere-2025-2698
Preprint. Discussion started: 3 July 2025

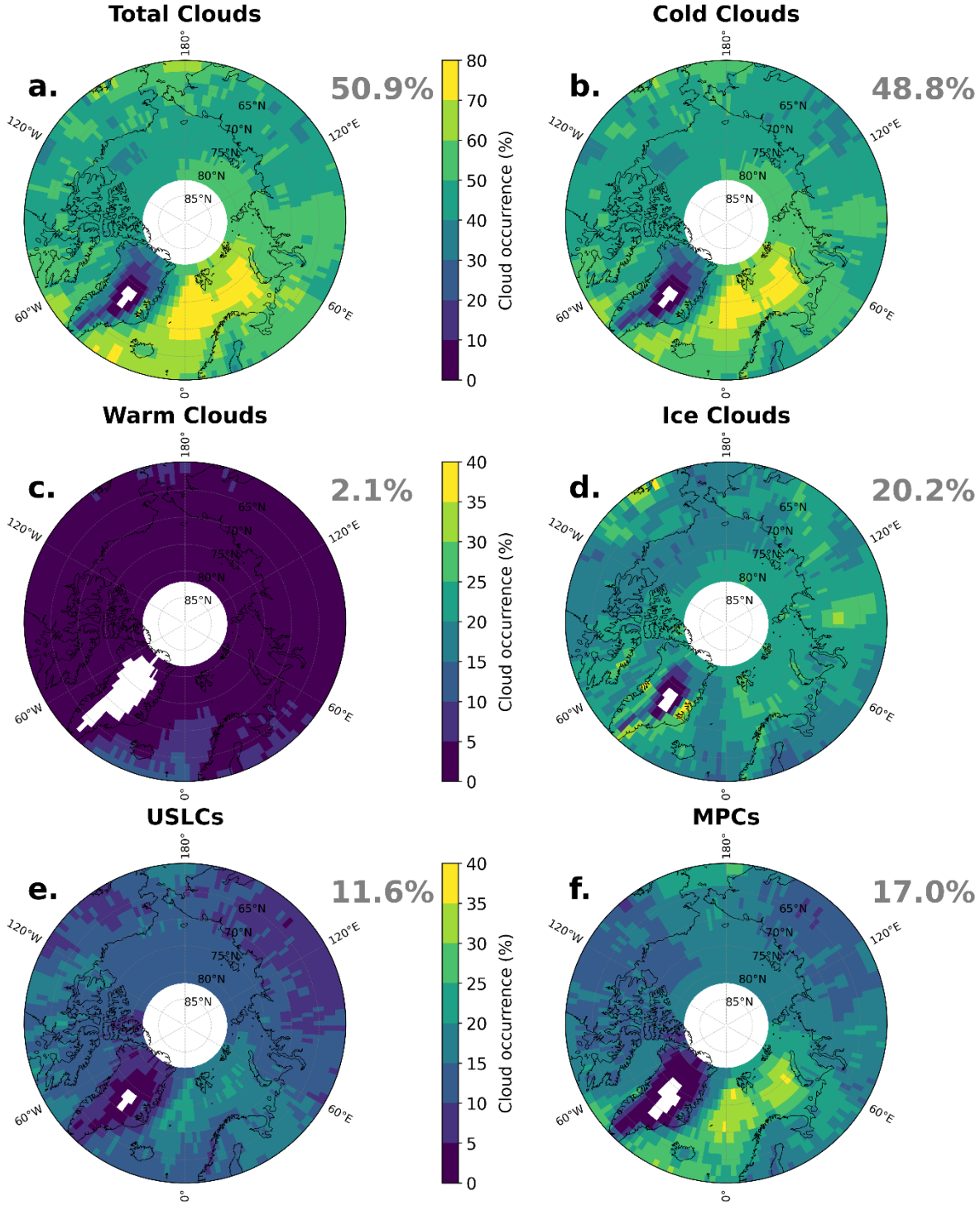

https://doi.org/10.5194/egusphere-2025-2698
Preprint. Discussion started: 3 July 2025

Figure 1. Stereographic projections of the occurrence of low-level (0.5-3 km) cloud types between 2007 and 2016: (**a**) total clouds, (**b**) cold clouds, (**c**) warm clouds, (**d**) ice clouds, (**e**) USLCs, and (**f**) MPCs. The number in the upper right of each subfigure represents the median occurrence for the entire study area.

3.2 Seasonal variability of low-level cloud occurrences

Regional and seasonal variations between Arctic sub-regions are illustrated in **Figure 2.** The monthly variations of six representative Arctic regions are discussed below. The total low-level cloud occurrence shows clear inter-regional differences. The annual cycle follows a bimodal distribution as previously shown by Eastman & Warren (2010) and Shupe et al. (2011) with ground-based data. The same distribution has been observed with passive satellite data (Boccolari and Parmiggiani, 2018; Wang et al., 2021; Liu et al., 2023), active satellite data (Jiang et al., 2024), and ground-based sites (Shupe et al., 2011). Kay and L'Ecuyer (2013) and Arouf et al. (2024) also found a bimodal distribution of the surface longwave cloud radiative effect (LW CRE) over the Arctic region. The first peak occurs in May during spring [MAM], when low-level clouds are present 50% of the time in the Arctic (**Fig. 2b**, dashed black line). The second peak occurs in autumn with a larger amplitude reaching 60% and lasts for two months (Sept.-Oct.). This double seasonal peak of high cloudiness seems to occur in almost all Arctic regions except those influenced by the North Atlantic Ocean. For example, the Svalbard region (2A) has higher and more constant occurrences (60-70% throughout the year). Specific meteorological conditions at the regional scale are likely to explain these seasonal variations.

The first seasonal peak in spring could be related to the weakening of the tropospheric polar vortex at the end of winter. At this time of the year, the polar vortex disintegrates due to spring warming and interactions with atmospheric waves. This destructuring leads to thermal exchanges between mid-latitudes and high latitudes (Wu and Ovchinnikov, 2022; Murray-Watson et al., 2023). The change in atmospheric circulation with the upwelling of warmer air intrusions and moisture from the south could affect cloud occurrences (Kay and Gettelman, 2009; Morrison et al., 2018). During late winter, the region is subject to an increase in aerosol concentrations, the so-called "Arctic haze" (Law et al., 2014; Abbatt et al., 2019; Willis et al., 2019). This increase affects the radiation balance by modifying the distribution of aerosols and interacting with the formation of Arctic clouds. The second peak in autumn could result from changing surface conditions. These include more open water caused by sea ice melting since summer, reaching its maximum in autumn. In addition, the closer coupling of the ocean and atmosphere during non-summer seasons enhances low-level cloud formation over open water (Kay and Gettelman, 2009; Morrison et al., 2018). During this period of maximum sea ice breakup, the ocean brings more moisture into the atmosphere, favoring the formation and maintenance of low-level clouds (Stroeve et al., 2012; Morrison et al., 2019; Yu et al., 2019). These patterns are more pronounced in regions north of 70°N, particularly in the Eastern Arctic (2F) and Northern Canada (2D). In region 2F, the second maximum of cloud occurrence peaks at almost 80% in autumn. This peak is also well marked over the Bering Sea (80%) in November. This region is influenced by the Beaufort Gyre and experiences a later return of the ice pack. In the Svalbard region (2A), the local spring maximum can still be observed, but the second peak seems to develop later in early winter (December). In this region, the low-level cloud occurrence is higher than 50% throughout the autumn, winter, and spring seasons. During the summer, low-level cloud cover is at a minimum in all regions. More frequent high-

https://doi.org/10.5194/egusphere-2025-2698
Preprint. Discussion started: 3 July 2025

330 pressure systems over continents and increased instability from rising ocean temperatures likely explain this pattern. Mioche et al. (2015) showed that on average, summer clouds are more frequent at higher altitudes (between 3 km and 6 km) than at lower altitudes.

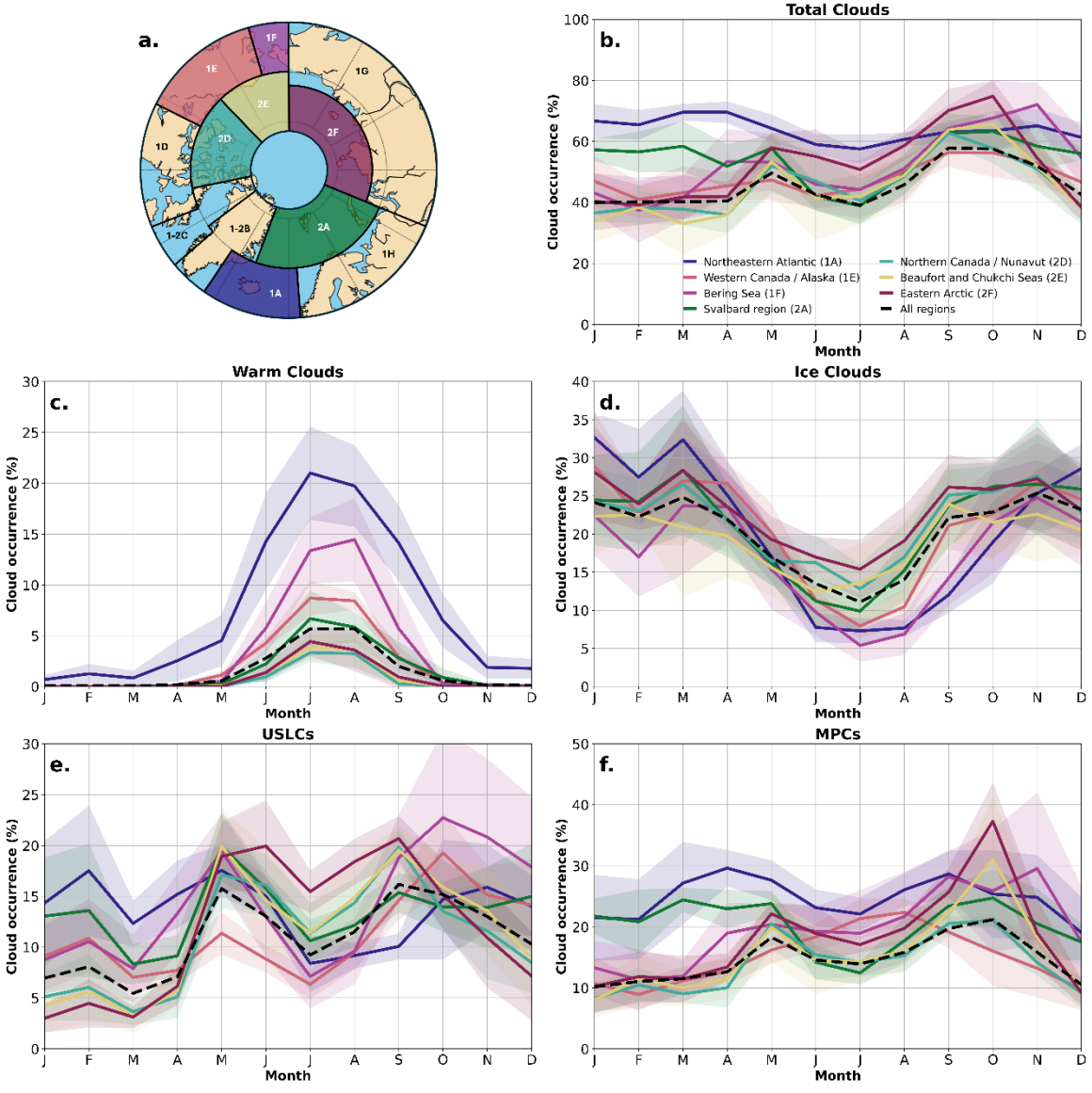

Figure 2. Monthly occurrence variations for different types of low-level clouds between 2007 and 2016: (**b**) total
335 clouds, (**c**) warm clouds, (**d**) ice clouds, (**e**) USLCs, and (**f**) MPCs. Regionalization (**a**) with colored regions for monthly analysis. The colored areas around the curves represent the interquartile range. Zone 1 represents the low

https://doi.org/10.5194/egusphere-2025-2698
Preprint. Discussion started: 3 July 2025

latitude regions from 60°N to 70°N, excluding the Russian continental region. The letters for the different regions start from the North Atlantic zone (1A) and run from west to east. Zone 2 is the second high latitude ring, from 70°N to 82°N. Regions in this latitude band are referred to in the same way as the first ring.

Figure 2c shows the monthly variations of warm cloud occurrences (OC_{warm}). Warm liquid clouds are absent in winter, autumn, and early spring, except in region 1A. In summer, the median OC_{warm} over all regions reaches its highest value in July but remains moderate at only 6%. Lower latitude regions (1A, 1E, and 1F) exhibit higher OC_{warm} (> 10%) compared to higher latitude regions (2A, 2E, and 2F), where warm low-level clouds are observed only 5-6% of the time. A maximum frequency of occurrence of 20% is observed over the Northeast Atlantic regions (1A) in July. In all regions, the occurrence of ice clouds (OC_{ice}, **Fig. 2d**) peaks in winter. It then decreases until July before rising again in autumn. OC_{ice} seems to follow a monomodal distribution opposite to that of warm clouds. Colder conditions favor the prevalence of ice clouds (median OC_{ice} up to 24% over the whole Arctic in winter). Over the Northeast Atlantic (1A) and the Western Arctic (not shown here), low-level ice clouds are more frequent during this season (OC_{ice} >30%). In summer, the occurrence is minimal (median around 11%) and ranges from 5% over the Bering Sea (1F) and the North Atlantic (1A) to 16% over the Arctic Seas north of Siberia (2F). During this season, ice clouds are more frequent in high-latitude regions (2A, 2D, and 2F). In contrast, warm liquid clouds occur mainly in the low-latitude Arctic regions, as discussed above. Warm clouds and ice clouds have opposite monthly variations driven by the meridional transport of heat and moisture. These cloud types can be considered as seasonal clouds as their occurrences seem to be strongly influenced by the latitudinal temperature.

The temporal evolution of the frequency of occurrence of USLCs (OC_{USLCs}) and MPCs (OC_{MPCs}) is close to that characterizing total clouds. **Figures 2e** and **2f** show that the first peak occurs in spring and the second in autumn. The two seasonal peaks of OC_{USLCs} seem to have the same values, close to 15%. A comparison between regions suggests a certain homogeneity of OC_{USLCs} during peak periods. Some regional inhomogeneities are observed, with high-latitude regions (2D and 2E) showing low OC_{USLCs} in winter, below 5%. In summer, these regions experience higher USLCs occurrences, reaching up to 20% in 2F. The two seasonal occurrence peaks are visible (**Fig. 2f**) when the MPCs are investigated at the scale of the whole Arctic domain. The first one reaches 18% in late spring, while the second peak of OC_{MPCs} is stronger with a median value close to 25% in autumn. The monthly distribution of OC_{MPCs} also shows strong regional differences. During winter and early spring, regions influenced by the heat and moisture transport of the Atlantic Ocean (1A and 2A) show the highest occurrences of MPCs (up to 30% median occurrence for region 1A). For these seasons, the western and eastern Arctic regions are characterized by lower-than-average MPCs occurrence values (10-15%). The inter-regional differences are even greater in autumn when the second peak occurs. For example, MPCs are present more than 40% of the time in the 2F region, compared to 20% in northeastern Canada (2D). The presence of mixed-phase clouds seems to be determined by many factors.

3.3 Linking cloud-type occurrence to environmental conditions using multilinear regressions

3.3.1. Regional environmental conditions

https://doi.org/10.5194/egusphere-2025-2698
Preprint. Discussion started: 3 July 2025

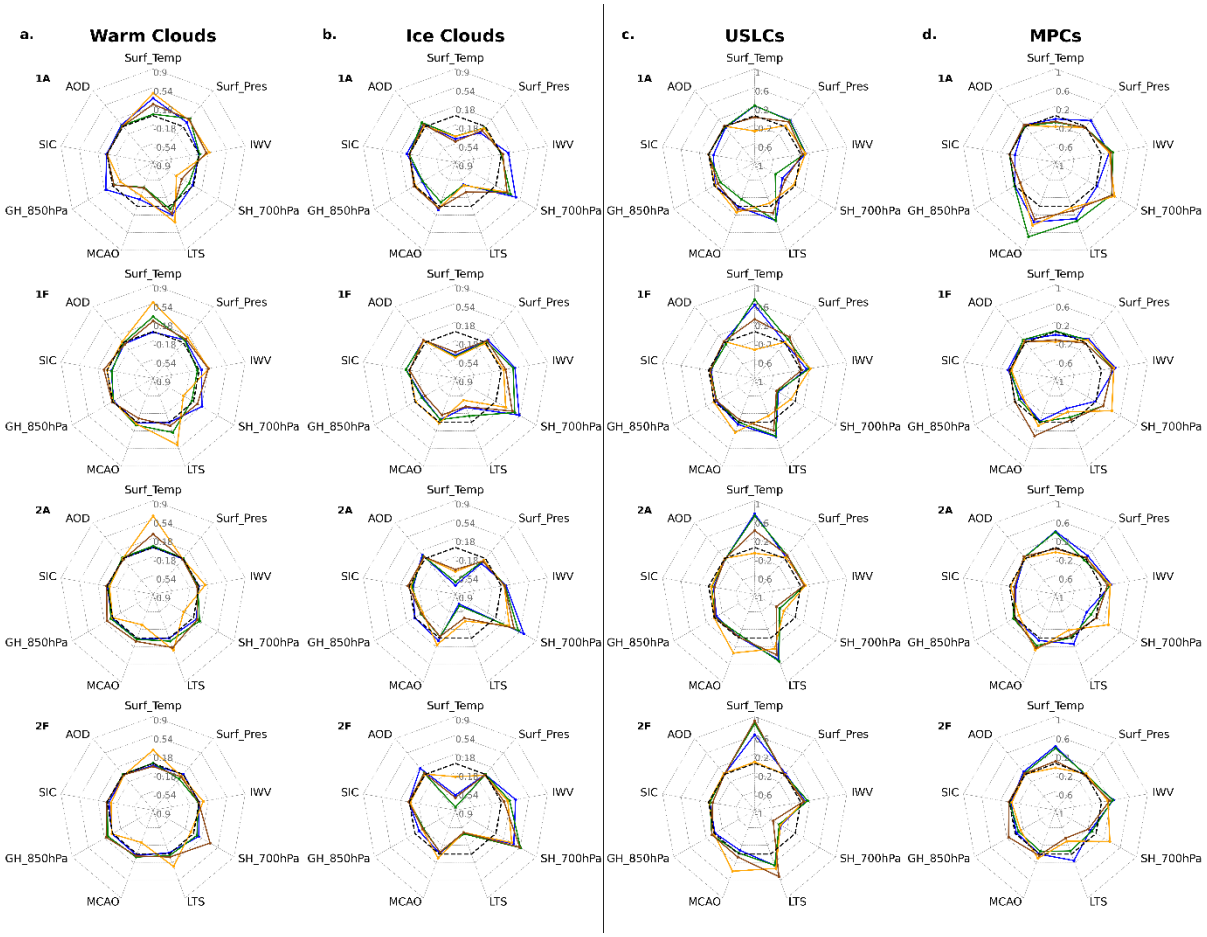

Figure 3. Normalized coefficients of MLR for low-level (**a**) warm clouds, (**b**) ice clouds, (**c**) USLCs, and (**d**) MPCs for 4 regions (1A, 1F, 2A, and 2F) during 4 seasons: (blue) winter, (green) spring, (orange) summer, and (brown) autumn. The dashed black line corresponds to the value zero.

In the following, we propose to investigate and quantify the specific influence of a set of environmental parameters (thermodynamics and surface conditions) on cloud occurrences with analyses based on multiple linear regressions (MLR). The full methodology and coefficients associated with the MLR are provided in Appendix B. The MLR presented below was implemented using nine variables: surface temperature (Surf_Temp), surface pressure (Surf_Press), integrated water vapor (IWV), Lower-Tropospheric Stability (LTS), Marine Cold Air Outbreak (MCAO), specific humidity at 700 hPa (SH_700hPa), geopotential height at 850 hPa (GH_850hPa), sea ice concentration (SIC), and aerosol optical depth (AOD). **Figure 3** shows the normalized MLR coefficients for the four cloud types (warm, ice, USLCs, and MPCs) for selected and contrasted regions (1A, 1D, 2A, and 2F). These four regions have been chosen as examples to highlight the differences in surface area (pack ice, o ceanic, and continental) and for different latitudes.

https://doi.org/10.5194/egusphere-2025-2698
Preprint. Discussion started: 3 July 2025

The MLR analysis shows that 3 parameters explain most of the variability in cloud occurrences. Surface temperature is anti-correlated with OC_{ice} and positively correlated with OC_{warm} and OC_{USLCs}. The impact of LTS generally follows the same trend as surface temperature. More stable conditions are associated with larger liquid cloud occurrences. Specific humidity at 700 hPa is positively correlated with OC_{ice} and negatively correlated with OC_{warm} and OC_{USLCs}. **Figure 3a** shows that warm liquid clouds are mainly associated with warm surface temperature, strong inversions (high LTS, stable conditions), and humidity. These thermodynamic conditions favor the occurrence of low-level warm clouds, especially in summer. The same patterns are observed at low latitudes (regions 1A and 1F) but are less obvious in the Eastern Arctic region (region 2F). Low-level warm cloud occurrences are poorly represented by the MLR in high-latitude regions due to their low number of data. The analysis is therefore more robust for region 1A, which has the highest occurrences. The negative coefficient of SH_700hPa and the positive coefficient of the LTS indicate that liquid clouds seem to be more likely influenced by the lower layers (Morrison et al., 2019; Taylor & Monroe, 2023). Negative values of the MCAO on the OC_{warm} indicate that these clouds may be impacted by the WAI, especially during cold seasons. The MLR representing USLCs (**Fig. 3c**) generally shows the same pattern as OC_{warm}. However, the regressions show marked differences between summer and other seasons. During the summer period, USLCs would be influenced by cold temperatures favored by the MCAO combined with strong stability at high latitudes.

Ice clouds (**Fig. 3b**) tend to occur more often over colder, wetter, and less stable lower atmospheric layers. However, specific humidity at 700 hPa appears to have a significant impact on the seasonal and spatial distribution of ice clouds. The presence and supply of moisture at altitude seem to be a key factor in the presence of ice clouds. Ice crystals nucleate at the top of the cloud (Rangno and Hobbs, 2001). This is also why GH_850hPa and MCAO impact these clouds, as they characterize the air mass. OC_{ice} seems to be favored by high AOD during winter at high latitudes (2D and 2F), with the intrusion of polluted air masses having a direct impact on the concentration of IN (Koike et al., 2019; Coopman and Tan, 2023).

Figure 3d shows the normalized coefficients of the MLR for MPCs across four seasons. The models representing the occurrences of MPCs show a pronounced inhomogeneity, both between regions and between seasons. It is challenging to determine whether this is a representativity issue with the models or whether the OC_{MPCs} are influenced by a multitude of factors depending on the season. Surface temperature, LTS, and specific humidity remain important parameters for the regression variability. The MCAO parameter has a very strong influence on oceanic regions (1A, 1F, and 2A) for all seasons. Sea ice concentration tends to reduce the presence of mixed-phase clouds (Cesana et al. 2023). However, the contribution of sea ice concentration appears to be small compared to the other parameters. This is in contrast to sea surface pressure and integrated water vapor content, which would favor the formation and persistence of this type of cloud. As with the occurrences of other clouds, a pattern is observed between regions during the summer. It is also during the summer season that the regressions best represent mixed-phase clouds.

3.3.2 Key environmental factors controlling the cloud-type distribution

Figure 4 shows the most influential MLR ($R^2 > 0.2$) coefficient for all seasons for the different cloud types. This section is related to the study by Naud et al. (2023) and Scott et al. (2020), who carried out the same work

https://doi.org/10.5194/egusphere-2025-2698
Preprint. Discussion started: 3 July 2025

but at a low latitude (< 60°). The regressions are performed for each grid point (2° latitude by 2° longitude). The analysis conducted for each season is shown in **Figure S3** in Supporting Information. In line with the regional regressions, surface temperature, MCAO, LTS, and specific humidity are the most influential parameters. They account for most of the cloud occurrence variability observed in lower latitude continental regions (regions 1G, 1E, and 1D, **Fig. 4**).

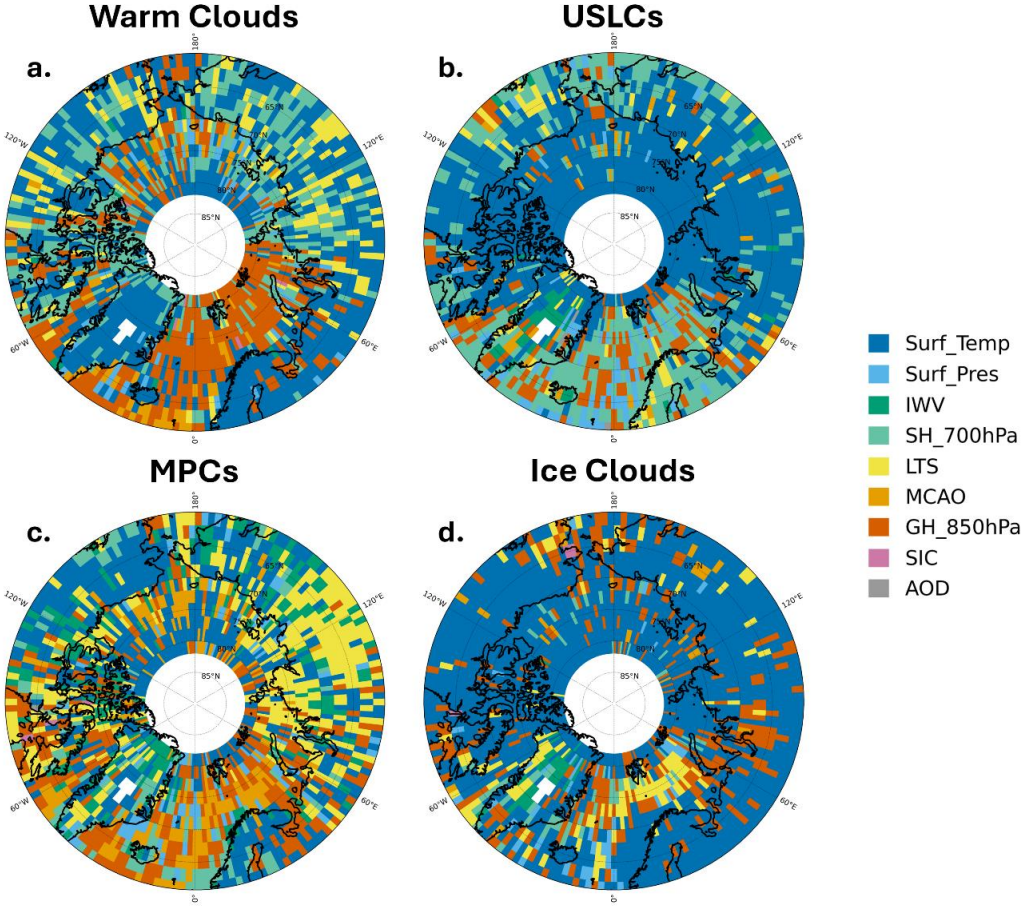

Figure 4. Most influential parameters of MLR for low-level (**a**) warm clouds, (**b**) USLCs, (**c**) MPCs, and (**d**) ice clouds for all seasons. The most influential parameter is only selected if the MLR has an $R^2 > 0.2$.

A comparison of the dominant parameters between the different cloud types shows significant results. Oceanic regions (such as 1A, 1F, and 2A) remain areas of interest, especially due to the high variability of the most influential parameters. For example, the Svalbard region (2A) or the Bering Strait (1F) show variations in the most influential parameters depending on the cloud type. Surface temperature is the main factor impacting the OC_{USLCs} and OC_{ice} (**Figs. 4b** and **4d**), especially for continental regions (1D and 1G). Over oceanic regions,

https://doi.org/10.5194/egusphere-2025-2698
Preprint. Discussion started: 3 July 2025

specific humidity is the most influential parameter for OC_{USLCs}, particularly in autumn (**Fig. S3**, in Supporting Information). The supply of humidity at high altitude seems to be essential to maintain saturation in the ice and liquid phases. OC_{ice} shows a dependence on the LTS over the Svalbard region (2A). This influence (negative correlation) shows that the ice clouds develop and maintain themselves with lower stability and a contribution of moisture at higher altitudes. **Figure 4a** shows that the GH_850hPa is the most important parameter that influences the OC_{warm} over the oceanic region. The strong influence of the geopotential height (positive coefficient) on OC_{warm} shows that these clouds need a warm air mass to develop. **Figure 4c** shows the most influential groups of parameters on OC_{MPCs}. MPC occurrences over the continental region of Russia (1G) are mainly influenced by the LTS. In contrast, in oceanic regions like Svalbard (2A), MCAO has a strong impact on OC_{MPCs}. MCAO seems to have a greater influence during the transitional seasons (spring and autumn). As mentioned in the previous section, the OC_{MPCs} seem to be influenced by a variety of factors with local variability. It is important to note that SIC and AOD do not appear to be dominant parameters to explain the occurrence of different cloud types.

4. Discussion

This study investigates the spatial and seasonal variability of low-level Arctic clouds (500–3000 m) using eight years of DARDAR (CALIPSO–CloudSat) observations. Our results confirm the widespread presence of tropospheric clouds across the Arctic, with an average occurrence close to 70%. This average value is in agreement with previous studies based on 8 years of CALIPSO-CloudSat observations. Mioche et al. (2015) and Cesana et al. (2024) used DARDAR-MASK products to show that tropospheric clouds were detected on average more than 70% and 77% of the time, respectively. Matus and L'Ecuyer (2017) analyzed 2B-CLDCLASS-LIDAR cloud phase classification products to obtain an annual cloud fraction of nearly 75% across the entire tropospheric column. Our estimates are also consistent with the cloud cover inferred from ground-based remote sensing observations ranges between 60 and 80% over western Arctic continental regions and Svalbard (Shupe et al., 2011).

Previous results on the occurrence of low-level clouds over the pan-Arctic are scarce and not explicitly addressed in most of the published studies despite their importance for the surface energy budget. We report a median occurrence of 51 (±3)%, which is higher than previous estimates based on AVHRR measurements where average values ranging from 35% to 57% were obtained (Philipp et al., 2020). However our result remains comparable to the 45-50% estimate derived from 14 years of CALIPSO-GOCCP observations reported in Jiang et al., 2024). We show that these low-level clouds exhibit strong geographical contrasts. They are more frequent over open ocean regions, especially in the North-East Atlantic and over the seas near the Svalbard archipelago (cloud occurrence of 64% and 54%, respectively) and less common over continental areas of Western Canada, Siberia, or the Beaufort Sea (42%) as previously mentioned by Mioche et al., 2015 and Jiang et al., 2024. Part of these differences can be explained by stronger cloud surface interactions over the open oceans (Gierens et al., 2020) favoring the vertical transfer of moisture, the formation and the persistence of clouds. In this respect, our results show that 48% of the low-level clouds are coupled to the surface in the Svalbard region compared to 17% over the Western Canada/ Beaufort Sea throughout the year (**Fig. S4** in Supporting Information).

https://doi.org/10.5194/egusphere-2025-2698
Preprint. Discussion started: 3 July 2025

Our results confirms that the low-level cloud occurrence follow a clear bimodal cycle, with maxima in spring and autumn. The first seasonal peak is most likely caused by a change in weather conditions at the end of winter (Yu et al., 2019). The high cloud cover observed in autumn is probably a consequence of changing surface conditions (Taylor & Monroe 2023; Cesana et al. 2024). Indeed, during this season, the maximum breakup of the pack ice facilitates the supply of moisture from below, which is favored by less stable conditions. Our results indicate that this seasonal pattern is more pronounced in northern regions of the Eastern Arctic and over the Bering Sea than over zones influenced by the Atlantic Ocean (northeastern Atlantic and Svalbard). High-latitude sea ice retreats more slowly than in southern regions, which affects the timing of the second seasonal peak (Yu et al., 2019). Recently, the work of Jiang et al. (2024) has also suggested similar regional specificity in the seasonal distribution of low-level clouds.

Our study is the first to investigate and quantify the seasonal and regional variability of the occurrence of four types of low-level clouds: warm liquid, ice-only, mixed-phase (MPCs), and unglaciated supercooled liquid clouds (USLCs). We show that warm and ice clouds exhibit opposite seasonal cycles, peaking in summer with a maximum occurrence of 10% for warm clouds and in winter, respectively. On the contrary, our results highlight that MPCs and USLCs follow bimodal distributions, peaking during the transitional seasons. We found a higher occurrence of low-level MPCs (17%) than earlier column-integrated estimates of 15% by Matus & L'Ecuyer (2017). We argue that compared to previous studies mixed-phase clouds are not limited to single mixed-phase layers but also include a combination of several successive liquid, mixed, and/or ice layers. We believe that this representation is more consistent with in situ observations (McFarquhar et al., 2007; Mioche et al., 2017, among others). Only a few studies have estimated the occurrence of low-level MPCs using ground-based remote sensing measurements. During the SHEBA campaign in the Beaufort Sea (2E region), Shupe et al. (2006) found an annual mean MPCs occurrence close to 40% with a maximum of 70% in September and a minimum of 10% in December. In the wider region (2E) encompassing the Beaufort Sea, our results show the same seasonal distribution, although the OC_{MPCs} are lower: an annual median value of 20%, an autumn maximum of 30%, and 9% in December. However, our estimates of MPCs occurrence over the Svalbard region (2A) are more consistent with the observations reported by Nomokonova et al. (2019) at the Ny-Ålesund station. Their results highlight a steep decline in MPCs occurrence from 25% in May to 5% at the beginning of summer, which is also observed in our study (25% in May and 12% in July). One of the innovative aspects of our study is the analysis of the regional distribution of USLCs. We find that the median occurrence of these clouds over the Arctic is about 12%. USCLs are frequent over oceanic regions where OC_{USLCs} are close to 15% but a maximum of almost 20% is reached at the end of spring and early autumn in the Eastern Arctic and over the Bering Sea. Taken together, liquid containing clouds (MPCs and USCLs) account for almost 60% of the low-level clouds. This point is in line with the findings of Cesana et al. (2012) based on 4 years of CALIOP lidar observations.

An innovative aspect of our study is the identification of environmental drivers of the regional and seasonnal distribution of low-level cloud type occurrence using multiple linear regressions. We found that the main parameters explaining cloud-type variability are surface temperature, lower-tropospheric stability (LTS), marine cold air outbreaks (MCAO), and specific humidity at 700 hPa. Warm clouds are favored by warm and stable conditions, while ice clouds are more common under cold, moist, and less stable environments. Over the regions

https://doi.org/10.5194/egusphere-2025-2698
Preprint. Discussion started: 3 July 2025

influenced by the North Atlantic Ocean (1A and 2A), the Bering Sea (1F), or the Baffin Bay (2C), the occurrence of MPCs is mainly correlated with the MCAO index, especially in spring and autumn. Previous studies have shown that air mass intrusions are expected to control cloud properties (Murray-Watson et al., 2023; Narizhnaya and Chernokulsky, 2024) and that thermodynamic changes associated with cold air outbreaks and warm air intrusions predominate for mixed-phase clouds (Woods and Caballero, 2016; Michaelis et al., 2022). In contrast, warmer temperatures and stable conditions also favor the USCLs coverage over the western and eastern Arctic which seems consistent with the study of Yu et al. (2019), suggesting that LTS exerts a strong influence on the liquid water paths of low-level clouds. An interesting result is that our analyses seem to indicate that in these regions, OC_{USLCs} are mostly associated with low geopotential height and lower specific humidity at 700 hPa. Contrary to MPCs, USCLs may be more frequent in the absence of transport of humidity from above (negative correlation with specific humidity at 700 hPa) and under more stable conditions.

Previous studies have highlighted the role of sea ice variability in modulating seasonal cloud cover and influencing microphysical and radiative cloud properties in the Arctic (Kay et al., 2016; Yu et al., 2019; Philipp et al., 2020; Wang et al., 2021; Cesana et al., 2024, among others). While our results confirm that sea ice concentration (SIC) exerts some influence—particularly during autumn when ice cover is most variable—they also indicate that thermodynamic parameters have a more substantial impact on cloud-type occurrences. Specifically, air temperature, lower-tropospheric stability (LTS), marine cold air outbreaks (MCAO), and mid-tropospheric humidity show stronger correlations with cloud presence than the extent or breakup of the sea ice pack. These thermodynamic drivers are naturally linked to surface conditions and to heat and moisture exchanges, which complicates the isolation of their individual effects. Nevertheless, our analysis suggests that the relationship between SIC and cloud occurrence is highly dependent on the spatial scale and methodology used. For instance, when applying simple linear regressions restricted to grid cells with varying sea ice fractions, we observe clearer anti-correlations between SIC and liquid clouds. In this case, SIC also appears positively correlated with ice clouds, with Spearman's rank correlation coefficients being highest in autumn (**Fig. S5** in Supporting Information). Despite these relationships, the overall correlations between SIC and cloud types remain weaker and more variable than those observed for LTS, temperature, or MCAO. This strengthens the hypothesis that the thermodynamic structure and air mass properties are the primary controllers of the regional Arctic low-level cloud variability, a result that aligns with the findings of Cesana et al (2024).

5. Conclusion

This study presents a detailed characterization of low-level Arctic clouds using eight years of CALIPSO-CloudSat observations coupled with refined cloud-type classification program (DARDAR-SOCP). We provide regionally robust statistical estimates of low-level cloud occurrences for different types of clouds. The results confirm the ubiquity of tropospheric clouds in the Arctic, with low-level clouds (500–3000 m) occurring 51% of the time. These clouds exhibit spatial and seasonal contrasts :

- The occurrence of warm liquid clouds and ice clouds is characterized by a monomodal distribution, with a summer peak for warm clouds (10%) and a winter peak for ice clouds (25%). Warm clouds are present

https://doi.org/10.5194/egusphere-2025-2698
Preprint. Discussion started: 3 July 2025

less than 3% of the time over the Arctic region, with a stronger presence at lower latitudes, especially over the northeastern Atlantic, where their occurrence reaches 10%. On an annual average, low-level ice clouds occur 20% of the time over the Arctic. They are more common at higher latitudes and over continental areas. For example, the ice cloud occurrence is greater than 30% over Alaska, central Siberia, and the coasts of Greenland.

- Clouds containing supercooled liquid droplets—Mixed-Phase Clouds (MPCs) and Unglaciated Supercooled Liquid Clouds (USLCs)—dominate the low-level cloud population, representing 60% of the low-level cloud. A major contribution of this work lies in the first satellite-based assessment of USLCs over the Arctic. These clouds, composed solely of supercooled liquid water droplets, represent on average 12% of low-level clouds, reaching up to 20% in certain oceanic regions during the transition seasons. Over the Arctic, the median occurrence of MPCs is 17%, reaching up to 40% over the Svalbard archipelago. Their spatial distribution and seasonal bimodal cycle exhibit strong regional dependencies. Both MPCs and, to a lesser extent, USLCs prevail over oceanic regions, especially in the North-East Atlantic sector, around Svalbard, and in the Bering Seas, where the occurrence of oceanic MPCs exceeds 20% in spring and 25% in autumn, while oceanic USLCs reach nearly 15%.

- Using multiple linear regression (MLR), we identify the dominant thermodynamic drivers of each cloud type. Surface temperature, lower tropospheric stability (LTS), marine cold air outbreaks (MCAOs), and mid-tropospheric humidity (at 700 hPa) emerge as the most influential variables. Notably, USLCs appear to be more sensitive to stable conditions and lower mid-tropospheric humidity, in contrast to MPCs, which are often associated with more pronounced air mass movements such as MCAOs, particularly during the transition seasons and over oceanic regions.

- The impact of sea ice concentration (SIC) on cloud occurrence is found to be secondary, with its influence generally weaker than that of thermodynamic parameters. This reinforces the idea that meteorological conditions—not SIC alone—govern the formation and maintenance of Arctic low-level clouds.

This study highlights important directions for future research aimed at refining our understanding and representation of Arctic low-level clouds. First, incorporating additional dynamic and thermodynamic variables—such as wind patterns, vertical velocity, and temperature advection—could provide a more complete picture of the processes driving cloud variability across regions and seasons. The role of aerosols, particularly their capacity to modulate cloud phase through microphysical interactions, remains an important aspect to explore, especially in relation to seasonal aerosol cycles in the Arctic. Further, our results highlight the need to better represent regional air mass characteristics, including geopotential height anomalies and marine air mass intrusions, which significantly influence the occurrence of both liquid and mixed-phase clouds. The DARDAR-SOCP classification approach developed here could be extended to new satellite missions like EarthCARE, enabling consistent monitoring of cloud phase distributions in a changing Arctic environment. More broadly, the detailed statistics and environmental dependencies established in this work provide a valuable basis for improving cloud

https://doi.org/10.5194/egusphere-2025-2698
Preprint. Discussion started: 3 July 2025

parameterizations in climate models, with implications for more accurate simulation of surface energy budgets and feedback mechanisms under Arctic amplification.

Appendix A: Comparison of 2007-2010 and 2013-2016 periods

For the first 4 years of data (2007-2010), the CloudSat satellite operated normally, sampling the atmosphere 10 to 15 seconds ahead of CALIPSO. In 2011, a battery problem on CloudSat led to a loss of synchronization with CALIPSO and operational problems with the CPR radar. CloudSat resumed joint observations with CALIPSO in 2012. However, technical problems necessitated the adoption of a new mode (Daylight Only Operations) for data from 2013 to 2016 (Braun et al., 2019; Listowski et al., 2019). During this second measurement period, CloudSat was only able to take atmospheric measurements during the daytime part of its orbit, for about 60 out of the 99 minutes of full orbit. As a result, about 40% of the scientific data could not be exploited (Kotarba and Solecki, 2021). This missing data concerns the nighttime period. Cloud climatology conducted using CloudSat data after 2012 shows a bias, particularly over the oceans (Noel et al., 2018). Data availability for this study is shown in **Fig A1b**.

a)

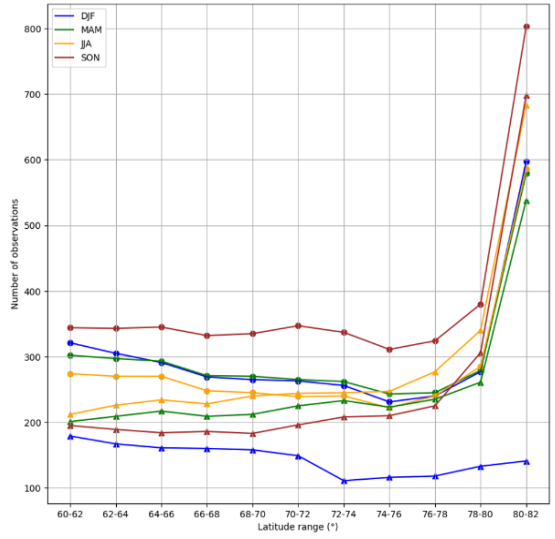

b)

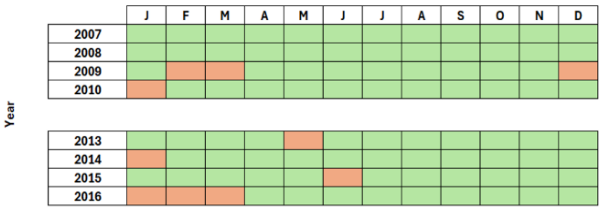

c)

	2007-2010		2013-2016	
	Total clouds	MPCs	Total clouds	MPCs
All seasons	51,39	18,87	51,44	17,72
DJF	42,29	12,89	43,71	12,63
MAM	47,11	15,78	49,06	16,41
JJA	46,58	18,58	48,04	17,72
SON	64,95	25,93	64,95	23,55

Figure A1. (a) Average number of observations per grid cell as a function of latitude for the 4 seasons (winter in blue, spring in green, summer in yellow, and autumn in brown). The circles represent the 2007-2010 period and the triangles the 2013-2016 period. Table **(b)** represents the availability of DARDAR mask v2.23 data for this study (green: available and orange: not available). Table **(c)** compares the average occurrences for the seasons between the 2 periods (2007-2010 and 2013-2016) for total clouds and MPCs.

A comparison of the average number of observations per grid cell as a function of latitude highlights the differences between seasons and periods (**Fig. A1a**). Overall, the number of observations is reduced by 30% for

https://doi.org/10.5194/egusphere-2025-2698
Preprint. Discussion started: 3 July 2025

low-latitude meshes (latitude < 66-68°) between the two periods due to daylight-only operation in 2013-2016, especially for winter and autumn. For summer and spring, this difference is much less pronounced, due to the polar day during these seasons. For high-latitude grids (latitude > 76-78°) the difference is very small in spring, summer, and autumn. Winter is the season with the largest discrepancy in the number of observations, especially for high-latitude meshes (latitude > 76-78°) due to the polar night. The last mesh (80-82°) loses up to 80% of the number of observations between the two periods. During the second period, observations are significantly reduced (especially in winter) for these meshes and, more generally, for high-latitude regions.

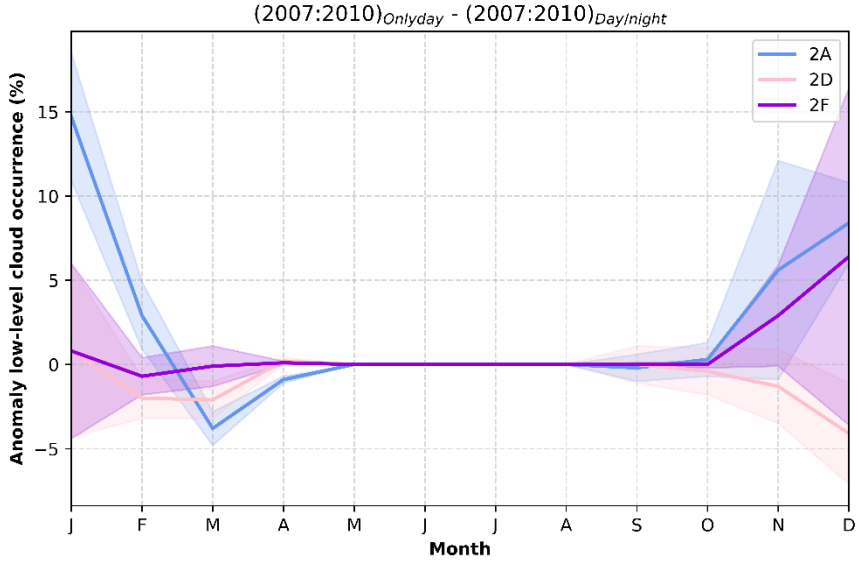

Figure A2. Cloud occurrence anomalies for 3 high-latitude regions (2A, 2D, and 2F) for the period 2007-2010 with two operating modes: day only and day/night. The colored curves represent the average values and the colored areas around the curves represent the standard deviation range.

Figure A1c compares the average occurrences over the two periods (2007-2010 and 2013-2016). A comparison between seasons shows that for total clouds, there seems to be no significant difference between the two periods. For example, there is a slight increase in average occurrences in winter for the period 2013-2016 (42.3% vs. 43.7%). This increase could be due both to the instrument malfunction and to the greater presence of clouds. The comparison for MPCs shows a slightly different behavior, with a seasonal decrease in occurrences over the period 2013-2016 (+1% for MAM vs. -2% for SON). **Figure A2** shows a comparison of occurrences for the period 2007-2010 (satellite instruments operational) using 2 operating modes (day only and day/night) for 3 high-latitude regions (affected by polar night). In terms of occurrences, the greatest differences are observed in December and January. However, these differences are larger for region Svalbard (2A) (**Fig. A2**) than for regions Eastern Arctic (2F) or Northern Canada/Nunavut (2D). The maximum difference for the Svalbard region (2A) is observed in January, with an average difference of 15% for all low-level clouds. In contrast, **Fig. A2** shows an underestimation of occurrences for the 2D region in early winter (November and December), but this remains

https://doi.org/10.5194/egusphere-2025-2698
Preprint. Discussion started: 3 July 2025

below 5%. As in Noel et al. (2018), it seems that the strongest anomalies are found over oceanic areas. Comparisons for other cloud types show maximum differences of 5% average occurrence during January. These differences appear to be consistently positive for daytime measurements, which means that there may be slight overestimation of cloud occurrences due to the CloudSat Daylight Only Operations mode over the period 2013-2016 for high-latitude regions during December and January.

Appendix B : Multiple linear regression

Multiple linear regressions (MLR) (Legendre and Legendre, 2012; Liu et al., 2021; Sharafi and Ghaleni, 2021) are used to explain the variation in a dependent variable (e.g., cloud occurrence) using several explanatory variables (e.g., meteorological parameters, sea ice concentration, and aerosol optical thickness). MLR is based on the least squares error estimator, fitting the model to the observations in such a way that the sum of the squares of the differences between the observed and predicted values is as small as possible. These regressions allow us to find the best model to represent the system or to evaluate the contribution of the explanatory variables to the dependent variable. The target variable (y) is defined from the explanatory variables (x_i) according to equation (1):

$$y = \beta_0 + \beta_1 x_1 + \cdots + \beta_i x_i + \epsilon \quad (1) \qquad\qquad \beta_i^{*} = \beta_i \frac{\sigma_{x_i}}{\sigma_y} \quad (2)$$

Where $\beta_i (i = 1,2, \dots, p)$ represents the regression coefficient for each explanatory variable. The first step in using MLR is to analyze the pairwise links between the explanatory variables $x_i (i = 1,2, \dots, p)$, β_0 corresponds to the intercept, y to the dependent variable, and ε to the model error. Equation (2) normalizes the coefficients of the MLR where $\beta_i^{*} (i = 1,2, \dots, p)$ represents the normalized coefficient, $\sigma_{x_i} (i = 1,2, \dots, p)$ represents the standard deviation of the explanatory variables, and σ_y represents the standard deviation of the dependent variable (Bring, 1994; Grace et al., 2018). This normalization allows coefficients to be compared with one another. The aim is to be able to identify any multi-collinearity between variables. The Variance Inflation Factor (VIF) is used to detect a potentially strong link between two variables (not shown). For a VIF value greater than 5, multicollinearity is too high, and the associated explanatory variable is removed from the MLR (Liu et al., 2021). The VIF is applied between thermodynamic parameters and clouds. Non-significant variables (i.e., those with a p-value greater than

https://doi.org/10.5194/egusphere-2025-2698
Preprint. Discussion started: 3 July 2025

0.05) were not retained for use in the different MLR. This discrimination is made before each MLR and set up for the different cloud types. These statistical parameters are shown in **Fig. B1**.

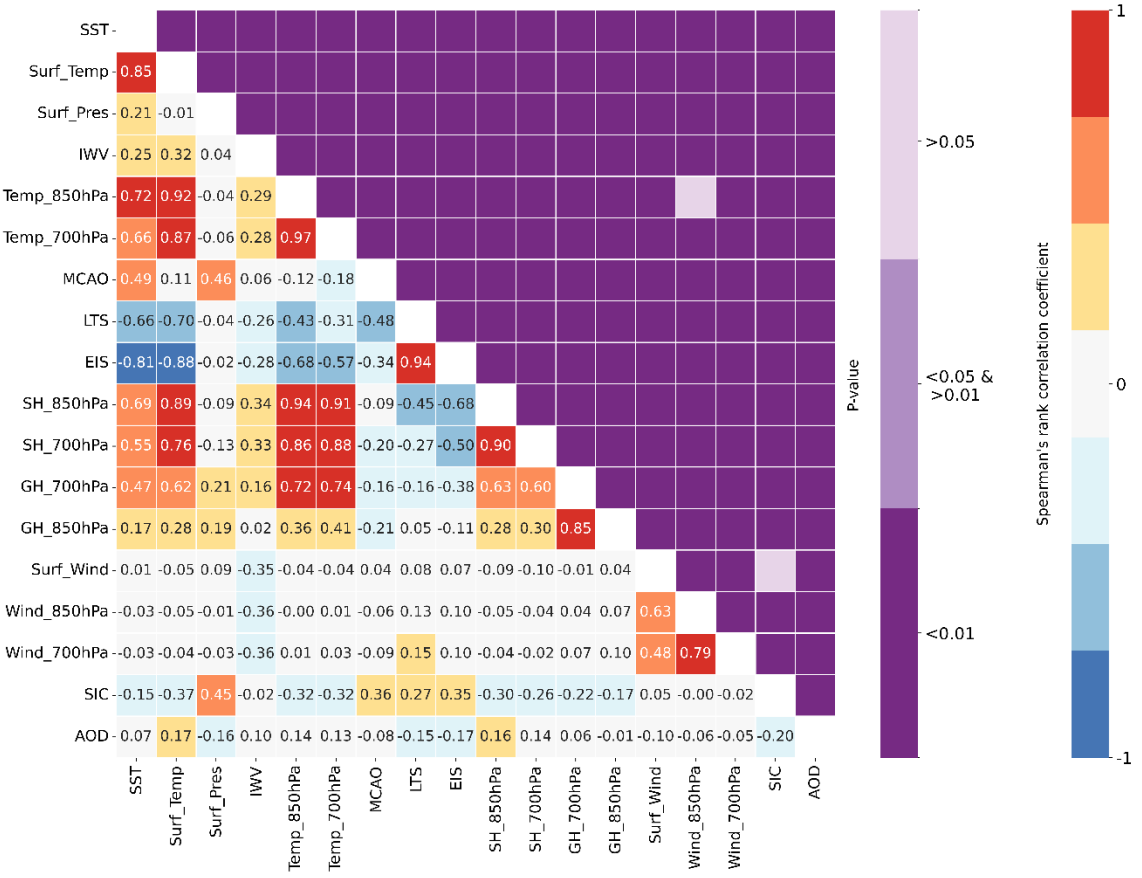

Figure B1. Spearman's rank correlations and p-value associated for each parameter for all regions.

In addition, the dataset undergoes a z-score test to remove outliers to further enhance the significance of the results. As the study covers 8 years of satellite measurements, the study area is represented by approximately 680,000 points. To ensure that each regression point is representative (as reminder, a regression point is the average on a 2° lat x 2° lon box over 7 days), tests were performed to highlight the number of observations per grid cell over 7 days in the study area. To avoid problems of representativeness for each regression point, a minimum observation threshold was chosen for the data at each latitude level. This minimum threshold corresponds to the first quartile of our dataset for each latitude. It allows us to exclude 25% of the points with the lowest number of observations and therefore the least statistically representative data points. Finally, the dataset was divided into two sets, the first (80% of the dataset) to train the models and the second (the remaining 20%) to test the models. 9 environmental parameters were used in the multiple linear regression: surface temperature (K), surface pressure (hPa), integrated water vapor between the surface and 1500 m (kg/m²), MCAO (K), LTS

https://doi.org/10.5194/egusphere-2025-2698
Preprint. Discussion started: 3 July 2025

(K), specific humidity at 700 hPa (g/kg), geopotential height at 850 hPa (m), sea ice concentration (%), and aerosol optical depth. These parameters were selected for their independence and importance for each region.

To quantify model error, the coefficient of determination (R^2 and adjusted R^2), root mean square error (RMSE), and the model bias are calculated and compared from the test dataset (**Tab. B1**). The coefficient of determination R^2 (eq. 3) measures the proportion of total variance explained by the model. This coefficient varies between 0 and 1, with a value close to 1 indicating that the model fits well the observed data. In a statistical model, the addition of an explanatory variable makes it possible to explain more variation even with an uncorrelated variable, a problem known as random fluctuation. The adjusted coefficient of determination overcomes this problem by taking into account the number of random variables and the size of the dataset. The coefficient of determination can be adjusted using equation (eq. 4). The root mean square error (RMSE, %) indicates the dispersion and variability of the model's prediction. This index represents the standard deviation of the residuals (eq. 5). It measures the accuracy of a model by evaluating the mean difference between actual and predicted values. Finally, model bias is a measure of the difference between model predictions and actual observations of the dependent variable (eq. 6). This index assesses whether the model tends to overestimate or underestimate the predicted values.

$$R^2 = 1 - \frac{\sum_{i=1}^{n} \hat{\epsilon}_i^2}{\sum_{i=1}^{n} (y - \bar{y})} \quad (3) \qquad adj.R^2 = 1 - \left(\frac{(n-1) \times (1 - R^2)}{n - k - 1} \right) \quad (4)$$

$$RMSE = \sqrt{\frac{1}{n} \sum_{i=1}^{n} (y - \hat{y}_i)^2} \quad (5) \qquad Bias = \frac{1}{n} \sum_{i=1}^{n} (\hat{y}_i - y_i)^2 \quad (6)$$

https://doi.org/10.5194/egusphere-2025-2698
Preprint. Discussion started: 3 July 2025

Cloud type	Region	Season	RMSE	R^2	adj.R^2	Surf_Temp		Surf_Pres		IWV		SH_700hPa		LTS		MCAO		GH_850hPa		SIC		AOD	
						β	β*	β	β*	β	β*	β	β*	β	β*	β	β*	β	β*	β	β*	β	β*
Ice Cloud	1A	Fall [SON]	16,5	0,36	0,36	-3,08	-0,50	-0,15	-0,10	0,24	0,03	5563,57	0,25	-1,65	-0,29	0,20	0,04	0,00	0,02	0,00	0,00	4,10	0,05
	1E		22,9	0,14	0,14	-1,61	-0,57	-0,08	-0,16	1,40	0,12	12731,13	0,41	-1,31	-0,31	0,16	0,05	-0,03	-0,12	-0,02	-0,01	2,96	0,04
	1F		20,6	0,17	0,17	-1,55	-0,40	0,10	0,05	0,84	0,08	10895,06	0,36	-1,82	-0,32	-0,64	-0,15	-0,06	-0,23	-0,01	-0,01	4,97	0,06
	2A		18,4	0,20	0,20	-1,45	-0,42	-0,12	-0,08	0,39	0,06	13418,51	0,40	-1,93	-0,41	-0,13	-0,03	-0,03	-0,15	0,02	0,03	3,81	0,04
	2D		20,1	0,16	0,15	-1,75	-0,66	-0,04	-0,05	1,03	0,14	29501,70	0,53	-1,73	-0,40	0,00	0,00	-0,02	-0,05	0,01	0,02	2,95	0,04
	2F		18,9	0,15	0,15	-1,70	-0,66	-0,02	-0,01	0,28	0,05	22803,17	0,53	-2,00	-0,44	-0,13	-0,04	-0,05	-0,18	0,01	0,02	2,92	0,03
	All regions		21,3	0,14	0,14	-1,40	-0,63	-0,07	-0,16	0,84	0,10	12263,10	0,37	-1,58	-0,43	-0,05	-0,02	-0,03	-0,22	0,00	0,00	4,32	0,05
	1A	Spring [MAM]	19,2	0,37	0,36	-3,28	-0,40	-0,06	-0,03	-0,03	0,00	11222,44	0,33	-2,68	-0,44	-0,42	-0,08	-0,05	-0,17	0,00	0,00	10,87	0,10
	1E		22,2	0,21	0,21	-1,44	-0,61	-0,08	-0,17	7,51	0,29	13328,11	0,36	-1,24	-0,32	0,08	0,03	-0,03	-0,13	-0,03	-0,03	4,18	0,05
	1F		23,2	0,21	0,20	-1,54	-0,48	0,05	0,02	6,00	0,23	18077,01	0,42	-0,67	-0,13	-0,20	-0,05	-0,05	-0,16	0,05	0,07	4,97	0,05
	2A		18,4	0,26	0,26	-1,94	-0,66	-0,09	-0,06	1,08	0,07	24588,82	0,50	-2,72	-0,66	-0,10	-0,03	-0,03	-0,14	-0,02	-0,05	6,01	0,06
	2D		19,2	0,18	0,18	-2,12	-0,89	0,00	0,00	3,16	0,17	30130,32	0,48	-1,94	-0,48	0,01	0,01	0,00	-0,01	-0,01	-0,03	2,52	0,03
	2F		16,9	0,22	0,22	-2,20	-0,84	0,00	0,00	2,17	0,16	29713,68	0,55	-1,93	-0,41	-0,10	-0,04	-0,04	-0,19	-0,01	-0,01	3,71	0,04
	All regions		21,4	0,17	0,17	-1,57	-0,70	-0,06	-0,12	3,00	0,15	16998,96	0,41	-1,64	-0,46	0,04	0,02	-0,03	-0,21	-0,04	-0,07	5,69	0,07
	1A	Summer [JJA]	8,5	0,26	0,25	-1,49	-0,40	-0,04	-0,04	0,08	0,02	2181,26	0,25	-1,46	-0,43	0,11	0,04	0,00	-0,01	0,00	0,00	0,50	0,02
	1E		11,6	0,30	0,30	-2,20	-0,85	-0,07	-0,23	0,83	0,12	2720,89	0,20	-1,80	-0,56	0,23	0,09	-0,01	-0,05	0,00	0,00	0,51	0,02
	1F		12,8	0,19	0,18	-1,93	-0,50	-0,04	-0,02	0,29	0,04	2996,86	0,22	-1,62	-0,45	0,06	0,02	0,00	-0,01	0,00	0,00	1,85	0,05
	2A		13,4	0,35	0,35	-2,29	-0,46	-0,08	-0,05	0,28	0,06	5958,71	0,30	-1,49	-0,35	0,47	0,14	-0,05	-0,18	-0,01	-0,02	2,05	0,04
	2D		14,3	0,35	0,35	-2,00	-0,41	-0,05	-0,09	0,97	0,18	7248,59	0,30	-2,02	-0,37	0,11	0,03	-0,06	-0,20	0,00	-0,01	0,03	0,00
	2F		14,2	0,31	0,31	-2,37	-0,26	-0,04	-0,02	0,54	0,12	8137,38	0,35	-2,09	-0,44	0,30	0,08	-0,05	-0,17	-0,01	-0,02	0,33	0,01
	All regions		13,4	0,33	0,33	-1,95	-0,78	-0,06	-0,16	0,60	0,11	3328,41	0,22	-1,63	-0,46	0,17	0,06	-0,03	-0,20	0,00	0,01	0,58	0,01
	1A	Winter [DJF]	21,4	0,24	0,24	-1,70	-0,45	-0,10	-0,16	4,36	0,14	19224,60	0,44	-2,06	-0,45	0,26	0,08	-0,02	-0,16	0,06	0,05	4,94	0,06
	1E		22,2	0,29	0,29	-1,58	-0,49	-0,07	-0,13	11,25	0,30	28026,71	0,52	-1,64	-0,37	0,19	0,08	-0,03	-0,10	-0,01	-0,01	5,46	0,06
	1F		21,5	0,25	0,25	-1,39	-0,46	0,13	0,07	9,70	0,26	25043,50	0,52	-1,20	-0,31	-0,15	-0,05	-0,04	-0,17	0,04	0,06	5,64	0,06
	2A		18,0	0,26	0,26	-1,87	-0,73	-0,18	-0,12	1,76	0,09	41076,41	0,62	-2,28	-0,70	0,15	0,05	0,00	0,01	-0,04	-0,08	10,41	0,09
	2D		17,7	0,24	0,24	-2,12	-0,59	-0,01	-0,02	6,29	0,29	47096,18	0,45	-2,20	-0,51	-0,03	-0,03	-0,01	-0,02	-0,01	-0,03	15,38	0,11
	2F		16,8	0,23	0,23	-2,23	-0,61	-0,01	-0,01	5,68	0,28	39097,19	0,40	-2,10	-0,42	-0,03	-0,01	-0,02	-0,10	0,01	0,01	26,34	0,15
	All regions		20,9	0,22	0,22	-1,73	-0,84	-0,03	-0,07	5,89	0,22	31936,10	0,50	-1,88	-0,65	0,03	0,02	-0,02	-0,14	-0,05	-0,09	10,81	0,11
Warm Cloud	1A	Fall [SON]	12,8	0,35	0,35	1,04	0,22	0,21	0,18	1,02	0,14	-4490,41	-0,26	0,67	0,15	-1,36	-0,38	0,00	-0,03	0,00	0,00	0,69	0,01
	1E		4,2	0,11	0,11	0,16	0,31	0,01	0,10	0,11	0,05	522,23	0,09	0,12	0,15	-0,02	-0,04	0,00	0,06	0,01	0,03	-0,01	0,00
	1F		7,0	0,17	0,16	0,27	0,20	0,06	0,09	0,62	0,18	872,28	0,09	0,14	0,07	-0,12	-0,08	0,00	0,01	0,04	0,06	-1,28	-0,05
	2A		5,8	0,13	0,13	0,27	0,26	-0,01	-0,02	-0,08	-0,04	823,03	0,08	0,27	0,19	0,07	0,07	0,01	0,12	0,00	0,01	-0,50	-0,02
	2D		1,1	0,02	0,02	0,03	0,19	0,00	0,02	0,01	0,04	2,79	-0,02	0,03	0,14	0,00	0,00	0,00	-0,01	0,00	-0,02	-0,06	-0,01
	2F		2,0	0,13	0,13	-0,02	-0,06	-0,01	-0,06	-0,01	-0,01	1682,77	0,37	0,03	0,06	0,01	0,04	0,00	0,14	0,00	0,00	-0,16	-0,02
	All regions		6,0	0,13	0,13	0,21	0,35	0,01	0,11	-0,02	-0,01	1011,12	0,11	0,24	0,23	0,00	0,01	0,00	0,10	0,00	-0,01	-0,36	-0,02
	1A	Spring [MAM]	9,5	0,17	0,17	0,10	0,03	0,17	0,20	0,07	0,01	-1495,96	-0,10	0,15	0,06	-0,87	-0,39	0,00	-0,03	0,00	0,00	1,05	0,02
	1E		1,9	0,12	0,12	0,08	0,41	0,00	-0,08	-0,16	-0,07	152,73	0,05	0,09	0,29	0,02	0,07	0,00	0,08	0,00	0,00	0,04	0,01
	1F		2,5	0,04	0,04	0,09	0,29	0,01	0,05	-0,09	-0,03	-162,41	-0,04	0,11	0,21	0,02	0,06	0,00	-0,01	-0,01	-0,10	-0,09	-0,01
	2A		2,5	0,03	0,03	0,01	0,03	0,00	0,01	-0,05	-0,03	774,75	0,13	0,03	0,06	0,01	0,02	0,00	0,04	0,00	-0,04	0,26	0,02
	2D		0,1	0,00	0,00	0,00	0,14	0,00	0,00	0,00	-0,02	-19,15	-0,05	0,00	0,08	0,00	0,00	0,00	-0,01	0,00	-0,01	0,00	0,00
	2F		0,3	0,01	0,01	0,00	0,01	0,00	-0,12	0,00	-0,02	63,10	0,07	0,00	0,03	0,00	0,06	0,00	0,11	0,00	0,00	0,00	0,00
	All regions		3,3	0,05	0,05	0,07	0,20	0,00	0,07	-0,04	-0,02	517,36	0,09	0,08	0,16	0,01	0,03	0,00	0,05	-0,01	-0,07	-0,27	-0,02
	1A	Summer [JJA]	19,1	0,30	0,29	3,72	0,43	0,34	0,17	1,81	0,20	-7847,66	-0,38	2,59	0,33	-1,41	-0,22	-0,06	-0,17	0,00	0,00	0,80	0,01
	1E		12,7	0,18	0,17	1,49	0,57	0,05	0,16	1,01	0,15	-1524,83	-0,11	2,46	0,76	0,55	0,22	0,00	0,00	-0,05	-0,05	-0,72	-0,02
	1F		16,9	0,23	0,23	2,98	0,57	0,27	0,13	1,67	0,19	-4239,34	-0,23	2,25	0,46	0,13	0,04	0,00	-0,01	0,00	0,00	1,25	0,02
	2A		11,6	0,31	0,31	2,51	0,61	-0,02	-0,01	0,52	0,12	-3697,21	-0,22	0,88	0,25	-0,78	-0,27	0,00	0,00	-0,02	-0,05	0,14	0,00
	2D		7,8	0,16	0,16	0,90	0,38	0,01	0,04	0,27	0,11	-616,32	-0,05	0,89	0,34	0,04	0,02	0,00	-0,01	-0,01	-0,06	-0,07	0,00
	2F		7,0	0,25	0,25	1,13	0,26	-0,04	-0,05	0,17	0,08	-666,71	-0,06	0,57	0,26	-0,42	-0,24	0,00	0,02	-0,01	-0,08	-0,58	-0,02
	All regions		13,4	0,21	0,21	1,50	0,66	0,04	0,12	0,72	0,14	-1842,35	-0,13	1,77	0,54	0,18	0,07	0,00	0,04	-0,04	-0,10	-0,32	-0,01
	1A	Winter [DJF]	6,1	0,12	0,12	0,33	0,33	0,02	0,11	0,00	0,00	-245,46	-0,02	0,22	0,18	-0,13	-0,14	0,01	0,15	0,00	0,01	0,99	0,04
	1E		0,3	0,02	0,02	0,01	0,22	0,00	0,01	0,00	-0,01	-73,71	-0,10	0,01	0,14	0,00	0,00	0,00	0,04	0,00	0,00	0,01	0,01
	1F		0.4	0,04	141,09	0,04	0,00	-0,01	0,00	0,06	0,03	0,05	0,19	0,00	0,00	0,00	0,02	0,00	-0,02	0,00	-0,08	-0,06	-0,04
	2A		0,2	0,00	0,00	0,00	0,00	0,00	-0,01	0,00	-0,01	33,32	0,06	0,00	0,00	0,00	0,02	0,00	0,02	0,00	-0,01	0,00	0,00
	2D		0,0	0,01	0,01	0,00	-0,05	0,00	0,00	0,00	-0,02	5,20	0,10	0,00	-0,03	0,00	-0,02	0,00	0,02	0,00	0,02	0,00	-0,01
	2F		0,1	0,01	0,01	0,00	-0,04	0,00	0,01	0,00	0,00	66,80	0,11	0,00	-0,02	0,00	0,03	0,00	0,01	0,00	-0,04	-0,02	-0,02
	All regions		1,6	0,02	0,02	0,02	0,12	0,00	0,06	-0,03	-0,02	269,84	0,06	0,01	0,06	0,00	-0,01	0,00	0,06	0,00	-0,02	0,07	0,01

https://doi.org/10.5194/egusphere-2025-2698
Preprint. Discussion started: 3 July 2025

Cloud type	Region	Season	RMSE	R^2	adj.R^2	Surf_Temp		Surf_Pres		IWV		SH_700hPa		LTS		MCAO		GH_850hPa		SIC		AOD	
						β	β*	β	β*	β	β*	β	β*	β	β*	β	β*	β	β*	β	β*	β	β*
MPCs	1A	Fall [SON]	22,2	0,18	0,17	-0,92	-0,13	-0,05	-0,03	2,30	0,21	10459,32	0,40	0,65	0,10	1,65	0,30	-0,03	-0,13	0,00	0,00	4,61	0,05
	1E		19,3	0,17	0,17	-0,95	-0,39	0,03	0,07	2,56	0,25	4798,17	0,18	-1,14	-0,31	0,30	0,11	-0,01	-0,03	-0,04	-0,04	2,02	0,03
	1F		25,0	0,16	0,15	-0,85	-0,18	-0,04	-0,02	2,77	0,23	6479,06	0,18	-0,37	-0,06	1,57	0,31	0,00	0,00	-0,01	-0,01	1,81	0,02
	2A		21,0	0,08	0,08	-0,09	-0,03	0,04	0,02	0,87	0,13	491,20	0,01	-0,30	-0,06	0,89	0,22	0,00	0,00	-0,07	-0,11	5,29	0,05
	2D		17,4	0,12	0,12	0,08	0,04	0,03	0,05	0,83	0,14	-3324,99	-0,07	-0,70	-0,19	0,15	0,08	0,00	0,01	0,01	0,01	3,08	0,04
	2F		18,7	0,23	0,23	0,13	0,05	-0,04	-0,03	1,01	0,18	-8448,42	-0,19	-1,72	-0,36	0,09	0,03	0,04	0,16	0,01	0,01	2,71	0,03
	All regions		20,7	0,16	0,16	-0,47	-0,22	0,05	0,11	1,35	0,17	2932,13	0,09	-1,15	-0,32	0,35	0,13	0,00	0,01	-0,04	-0,07	1,96	0,03
	1A	Spring [MAM]	21,4	0,29	0,28	-1,24	-0,14	-0,05	-0,02	5,84	0,24	13994,50	0,39	2,16	0,34	3,75	0,70	0,00	0,02	0,00	0,00	0,90	0,01
	1E		17,2	0,15	0,15	-0,33	-0,19	0,03	0,08	5,62	0,29	4154,34	0,15	-0,63	-0,21	0,05	0,02	-0,01	-0,07	0,01	0,01	2,76	0,05
	1F		21,0	0,14	0,14	0,03	0,01	0,12	0,07	5,33	0,23	6790,24	0,18	-0,50	-0,11	-0,02	-0,01	-0,03	-0,10	-0,02	-0,03	7,51	0,08
	2A		20,5	0,20	0,20	1,05	0,33	-0,08	-0,05	3,13	0,19	-6750,18	-0,13	-0,06	-0,02	0,62	0,17	0,01	0,04	-0,05	-0,10	3,82	0,03
	2D		14,2	0,26	0,26	0,59	0,32	0,07	0,13	3,84	0,27	-1086,27	-0,02	-0,43	-0,14	-0,14	-0,11	-0,03	-0,16	0,00	-0,01	4,76	0,07
	2F		14,5	0,22	0,22	0,72	0,32	0,00	0,00	2,80	0,24	-4636,21	-0,10	-0,29	-0,07	-0,13	-0,06	-0,02	-0,09	0,00	0,00	2,74	0,03
	All regions		18,8	0,21	0,21	0,14	0,07	0,04	0,08	4,24	0,24	505,76	0,01	-0,70	-0,22	0,08	0,04	0,00	-0,02	-0,03	-0,07	2,61	0,03
	1A	Summer [JJA]	21,8	0,28	0,28	-2,33	-0,24	-0,05	-0,02	1,79	0,17	10596,41	0,46	0,26	0,03	3,21	0,44	-0,05	-0,12	0,00	0,00	3,14	0,04
	1E		18,1	0,30	0,30	-2,33	-0,58	0,00	0,00	3,09	0,29	9884,31	0,47	-1,95	-0,39	0,34	0,09	-0,03	-0,12	-0,08	-0,05	0,57	0,01
	1F		20,4	0,28	0,28	-1,46	-0,22	0,18	0,07	2,89	0,27	9079,20	0,39	-1,43	-0,24	0,38	0,08	-0,09	-0,19	-0,07	-0,04	2,72	0,04
	2A		17,0	0,18	0,18	-0,55	-0,10	0,03	0,02	1,09	0,19	6854,08	0,31	-0,88	-0,18	1,03	0,27	-0,03	-0,10	-0,01	-0,02	0,56	0,01
	2D		14,8	0,20	0,19	-0,98	-0,21	0,06	0,10	1,01	0,20	7919,52	0,35	-1,22	-0,24	0,22	0,06	-0,04	-0,13	-0,01	-0,04	0,79	0,02
	2F		14,9	0,16	0,16	-0,83	-0,09	0,03	0,02	0,57	0,14	7515,82	0,34	-1,32	-0,29	0,36	0,10	-0,04	-0,14	-0,02	-0,05	0,52	0,01
	All regions		18,0	0,21	0,21	-1,62	-0,53	0,02	0,04	1,28	0,18	7954,98	0,43	-1,06	-0,24	0,71	0,20	-0,02	-0,16	-0,06	-0,11	0,51	0,01
	1A	Winter [DJF]	20,8	0,13	0,13	-0,25	-0,07	0,10	0,17	4,72	0,16	1065,83	0,03	1,19	0,28	1,11	0,36	0,00	0,00	-0,11	-0,12	3,69	0,05
	1E		16,1	0,11	0,11	-0,07	-0,04	0,00	0,01	5,72	0,23	-410,03	-0,01	-0,36	-0,13	0,03	0,02	-0,02	-0,14	-0,01	-0,02	3,84	0,07
	1F		20,0	0,19	0,19	-0,19	-0,07	0,16	0,10	9,70	0,30	-594,36	-0,01	-1,10	-0,31	-0,07	-0,03	-0,04	-0,15	0,02	0,03	6,28	0,07
	2A		18,7	0,17	0,17	0,87	0,35	0,10	0,07	4,01	0,21	-15092,97	-0,23	0,43	0,13	0,15	0,05	0,00	0,00	-0,06	-0,14	3,88	0,04
	2D		12,1	0,12	0,12	0,45	0,20	0,03	0,09	2,75	0,20	404,50	0,01	0,04	0,02	0,01	0,02	-0,01	-0,08	0,00	-0,02	6,96	0,08
	2F		11,6	0,16	0,16	0,89	0,37	-0,02	-0,02	3,47	0,26	-8844,65	-0,14	0,48	0,15	0,00	0,00	-0,01	-0,03	-0,01	-0,03	7,86	0,07
	All regions		16,3	0,20	0,20	0,43	0,27	0,03	0,10	4,45	0,21	-4803,75	-0,10	-0,10	-0,04	0,05	0,04	0,00	0,00	-0,04	-0,09	3,73	0,05
USLCs	1A	Fall [SON]	15,2	0,08	0,08	-0,16	-0,03	0,15	0,13	0,29	0,04	-4334,86	-0,25	0,66	0,15	0,25	0,07	-0,01	-0,09	0,00	0,00	0,79	0,01
	1E		19,1	0,12	0,12	0,74	0,32	0,03	0,06	1,50	0,15	-10986,79	-0,43	0,82	0,23	0,23	0,09	0,00	-0,02	-0,04	-0,04	1,33	0,02
	1F		21,5	0,12	0,12	1,04	0,26	0,31	0,15	0,20	0,02	-13972,13	-0,46	1,08	0,19	-0,23	-0,05	-0,01	-0,05	-0,06	-0,03	2,48	0,03
	2A		15,3	0,13	0,13	1,00	0,36	0,10	0,09	0,36	0,07	-12541,85	-0,47	1,44	0,38	-0,06	-0,02	0,00	-0,02	-0,06	-0,13	-0,76	-0,01
	2D		14,7	0,13	0,13	1,40	0,74	0,00	0,01	0,44	0,08	-18325,57	-0,46	1,09	0,35	0,06	0,04	-0,01	-0,04	-0,03	-0,08	0,68	0,01
	2F		13,7	0,19	0,19	1,74	0,91	-0,02	-0,01	0,24	0,06	-17380,56	-0,54	1,73	0,51	0,15	0,07	0,01	0,06	-0,03	-0,08	0,32	0,00
	All regions		17,2	0,13	0,13	1,02	0,57	0,03	0,09	0,65	0,10	-11899,68	-0,44	1,03	0,35	0,10	0,05	0,00	0,03	-0,05	-0,11	0,91	0,01
	1A	Spring [MAM]	15,3	0,20	0,20	1,27	0,22	0,23	0,16	1,68	0,10	-12000,38	-0,49	1,43	0,33	-0,60	-0,16	-0,03	-0,15	0,00	0,00	-0,93	-0,01
	1E		13,8	0,11	0,11	0,82	0,59	0,02	0,06	3,51	0,23	-7697,83	-0,35	0,88	0,38	0,04	0,02	0,00	0,01	0,00	0,01	0,59	0,01
	1F		19,1	0,20	0,19	1,80	0,69	0,16	0,10	3,95	0,18	-15468,03	-0,44	1,31	0,31	0,00	0,00	-0,01	-0,06	-0,02	-0,04	-4,04	-0,05
	2A		14,5	0,21	0,21	1,52	0,68	0,10	0,08	1,16	0,10	-14648,30	-0,39	1,67	0,53	-0,19	-0,07	0,00	-0,02	-0,02	-0,07	-1,52	-0,02
	2D		11,6	0,26	0,26	1,40	0,93	0,01	0,01	2,40	0,21	-16028,58	-0,41	0,87	0,34	-0,05	-0,05	-0,01	-0,06	-0,01	-0,05	0,45	0,01
	2F		12,1	0,29	0,29	1,67	0,85	-0,01	-0,01	1,55	0,15	-16079,38	-0,39	0,90	0,26	-0,04	-0,02	0,01	0,06	-0,01	-0,03	0,60	0,01
	All regions		14,3	0,19	0,19	1,25	0,83	0,02	0,06	2,34	0,18	-11338,15	-0,40	1,06	0,44	-0,04	-0,02	0,00	0,05	0,00	0,00	-0,25	0,00
	1A	Summer [JJA]	13,7	0,21	0,20	-1,91	-0,33	0,04	0,03	0,66	0,11	-512,28	-0,04	-0,37	-0,07	0,60	0,14	0,00	-0,02	0,00	0,00	0,46	0,01
	1E		12,1	0,25	0,25	-1,17	-0,45	0,01	0,04	0,86	0,12	-2074,66	-0,15	-0,28	-0,09	0,59	0,24	0,00	-0,02	-0,01	-0,01	1,16	0,04
	1F		14,0	0,25	0,24	-1,71	-0,39	0,02	0,01	1,52	0,21	-1641,05	-0,11	-0,59	-0,15	0,73	0,23	0,00	0,01	-0,03	-0,03	1,47	0,03
	2A		15,0	0,20	0,20	-0,60	-0,12	0,05	0,03	0,55	0,11	-5697,66	-0,28	1,04	0,24	1,16	0,34	0,00	0,00	-0,03	-0,06	0,07	0,00
	2D		14,2	0,15	0,15	-0,09	-0,02	0,04	0,08	0,46	0,10	-5617,35	-0,27	1,22	0,26	0,95	0,29	-0,02	-0,07	-0,03	-0,08	1,50	0,04
	2F		13,6	0,21	0,20	0,27	0,03	0,00	0,00	0,28	0,07	-7542,42	-0,37	1,38	0,33	1,31	0,39	0,00	0,01	0,00	0,00	1,18	0,03
	All regions		14,3	0,23	0,23	-0,73	-0,30	0,03	0,08	0,56	0,10	-3075,62	-0,20	0,40	0,11	0,88	0,31	-0,01	-0,08	-0,03	-0,06	1,49	0,04
	1A	Winter [DJF]	16,8	0,11	0,11	0,58	0,21	0,08	0,18	2,45	0,11	-9943,11	-0,32	1,10	0,33	0,03	0,01	0,00	-0,02	-0,08	-0,10	-1,79	-0,03
	1E		15,8	0,10	0,10	1,04	0,51	0,01	0,02	4,29	0,18	-11771,39	-0,34	0,91	0,33	-0,04	-0,03	0,00	-0,03	0,00	0,00	1,60	0,03
	1F		17,9	0,16	0,15	1,35	0,57	0,00	0,00	3,62	0,13	-15715,06	-0,42	1,01	0,33	0,11	0,05	-0,01	-0,04	-0,03	-0,06	1,77	0,02
	2A		14,2	0,16	0,16	1,37	0,72	0,04	0,04	1,35	0,09	-18937,27	-0,39	1,17	0,49	-0,05	-0,02	-0,01	-0,05	-0,04	-0,11	-1,60	-0,02
	2D		9,6	0,17	0,17	1,20	0,64	0,00	0,01	2,13	0,19	-17600,62	-0,33	0,77	0,34	-0,03	-0,05	-0,01	-0,06	0,00	-0,02	3,38	0,05
	2F		8,3	0,15	0,15	1,05	0,62	0,02	0,03	0,95	0,10	-16309,24	-0,35	0,60	0,26	-0,07	-0,08	0,00	-0,02	-0,01	-0,02	0,39	0,01
	All regions		13,4	0,18	0,18	1,13	0,88	0,00	0,01	1,97	0,12	-14483,93	-0,36	0,87	0,48	-0,02	-0,02	0,00	0,00	-0,02	-0,06	0,51	0,01

Table B1. The statistical measures for each MLR: adjusted R^2, R^2, RMSE, and normalized coefficients for each parameter.

https://doi.org/10.5194/egusphere-2025-2698
Preprint. Discussion started: 3 July 2025

Data availability. "DARDAR-MASK.v2.23" and "01kmCLay.v4.20" product products used for cloud phase retrieval and aerosol data in this study are available at https://www.icare.univ-lille.fr/ with free registered access. Sea ice concentration data from AMSR-E/AMSR2 satellite instruments are available at https://seaice.uni-bremen.de/sea-ice-concentration/amsre-amsr2/.

Competing interests. The authors declare that have no conflict of interest.

Author contribution. AD: Writing of the original manuscript, data processing, dataset analysis. GM: Edited the manuscript and analyzed the results. QC: Edited the manuscript and analyzed the results. CB: Methodology and data processing. JD: Methodology and manuscript editing. OJ: Edited the manuscript, analyzed the results, and supervised the project.

Acknowledgments. This work was funded by the Expecting Earth-Care Learning From A-Train (EECLAT, grant 6710) project financed by the Centre National d'Etudes Spatiales (CNES) and the (MPC)² project supported by the French Agence Nationale de la Recherche under the grant ANR-22-CE01-0009. The research used resources from the AERIS-ICARE National Atmospheric Data and Services Infrastructure.

References

Abbatt, J. P. D., Leaitch, W. R., Aliabadi, A. A., Bertram, A. K., Blanchet, J.-P., Boivin-Rioux, A., Bozem, H., Burkart, J., Chang, R. Y. W., Charette, J., Chaubey, J. P., Christensen, R. J., Cirisan, A., Collins, D. B., Croft, B., Dionne, J., Evans, G. J., Fletcher, C. G., Galí, M., Ghahreman, R., Girard, E., Gong, W., Gosselin, M., Gourdal, M., Hanna, S. J., Hayashida, H., Herber, A. B., Hesaraki, S., Hoor, P., Huang, L., Hussherr, R., Irish, V. E., Keita, S. A., Kodros, J. K., Köllner, F., Kolonjari, F., Kunkel, D., Ladino, L. A., Law, K., Levasseur, M., Libois, Q., Liggio, J., Lizotte, M., Macdonald, K. M., Mahmood, R., Martin, R. V., Mason, R. H., Miller, L. A., Moravek, A., Mortenson, E., Mungall, E. L., Murphy, J. G., Namazi, M., Norman, A.-L., O'Neill, N. T., Pierce, J. R., Russell, L. M., Schneider, J., Schulz, H., Sharma, S., Si, M., Staebler, R. M., Steiner, N. S., Thomas, J. L., Von Salzen, K., Wentzell, J. J. B., Willis, M. D., Wentworth, G. R., Xu, J.-W., and Yakobi-Hancock, J. D.: Overview paper: New insights into aerosol and climate in the Arctic, Atmospheric Chem. Phys., 19, 2527–2560, https://doi.org/10.5194/acp-19-2527-2019, 2019.

Achtert, P., O'Connor, E. J., Brooks, I. M., Sotiropoulou, G., Shupe, M. D., Pospichal, B., Brooks, B. J., and Tjernström, M.: Properties of Arctic liquid and mixed-phase clouds from shipborne Cloudnet observations during ACSE 2014, Atmospheric Chem. Phys., 20, 14983–15002, https://doi.org/10.5194/acp-20-14983-2020, 2020.

Arouf, A., Chepfer, H., Kay, J. E., L'Ecuyer, T. S., and Lac, J.: Surface Cloud Warming Increases as Late Fall Arctic Sea Ice Cover Decreases, Geophys. Res. Lett., 51, e2023GL105805, https://doi.org/10.1029/2023GL105805, 2024.

Bazantay, C., Jourdan, O., Mioche, G., Uitz, J., Dziduch, A., Delanoë, J., Cazenave, Q., Sauzède, R., Protat, A., and Sellegri, K.: Relating Ocean Biogeochemistry and Low-Level Cloud Properties Over the Southern Oceans, Geophys. Res. Lett., 51, e2024GL108309, https://doi.org/10.1029/2024GL108309, 2024.

https://doi.org/10.5194/egusphere-2025-2698
Preprint. Discussion started: 3 July 2025

Boccolari, M. and Parmiggiani, F.: Trends and variability of cloud fraction cover in the Arctic, 1982–2009, Theor. Appl. Climatol., 132, 739–749, https://doi.org/10.1007/s00704-017-2125-6, 2018.

Boisvert, L. N. and Stroeve, J. C.: The Arctic is becoming warmer and wetter as revealed by the Atmospheric Infrared Sounder, Geophys. Res. Lett., 42, 4439–4446, https://doi.org/10.1002/2015GL063775, 2015.

Bossioli, E., Sotiropoulou, G., Methymaki, G., and Tombrou, M.: Modeling Extreme Warm-Air Advection in the Arctic During Summer: The Effect of Mid-Latitude Pollution Inflow on Cloud Properties, J. Geophys. Res. Atmospheres, 126, e2020JD033291, https://doi.org/10.1029/2020JD033291, 2021.

Braun, B. M., Sweetser, T. H., Graham, C., and Bartsch, J.: CloudSat's A-Train Exit and the Formation of the C-Train: An Orbital Dynamics Perspective, in: 2019 IEEE Aerospace Conference, 2019 IEEE Aerospace Conference, Big Sky, MT, USA, 1–10, https://doi.org/10.1109/AERO.2019.8741958, 2019.

Bring, J.: How to Standardize Regression Coefficients, Am. Stat., 48, 209–213, https://doi.org/10.1080/00031305.1994.10476059, 1994.

Ceccaldi, M., Delanoë, J., Hogan, R. J., Pounder, N. L., Protat, A., and Pelon, J.: From CloudSat-CALIPSO to EarthCare: Evolution of the DARDAR cloud classification and its comparison to airborne radar-lidar observations, J. Geophys. Res. Atmospheres, 118, 7962–7981, https://doi.org/10.1002/jgrd.50579, 2013.

Cesana, G., Kay, J. E., Chepfer, H., English, J. M., and De Boer, G.: Ubiquitous low-level liquid-containing Arctic clouds: New observations and climate model constraints from CALIPSO-GOCCP, Geophys. Res. Lett., 39, 2012GL053385, https://doi.org/10.1029/2012GL053385, 2012.

Cesana, G., Chepfer, H., Winker, D., Getzewich, B., Cai, X., Jourdan, O., Mioche, G., Okamoto, H., Hagihara, Y., Noel, V., and Reverdy, M.: Using in situ airborne measurements to evaluate three cloud phase products derived from CALIPSO, J. Geophys. Res. Atmospheres, 121, 5788–5808, https://doi.org/10.1002/2015JD024334, 2016.

Cesana, G. V., Pierpaoli, O., Ottaviani, M., Vu, L., Jin, Z., and Silber, I.: The correlation between Arctic sea ice, cloud phase and radiation using A-Train satellites, Atmospheric Chem. Phys., 24, 7899–7909, https://doi.org/10.5194/acp-24-7899-2024, 2024.

Chepfer, H., Noel, V., Winker, D., and Chiriaco, M.: Where and when will we observe cloud changes due to climate warming?, Geophys. Res. Lett., 41, 8387–8395, https://doi.org/10.1002/2014GL061792, 2014.

Coopman, Q. and Tan, I.: Characterization of the Spatial Distribution of the Thermodynamic Phase Within Mixed-Phase Clouds Using Satellite Observations, Geophys. Res. Lett., 50, e2023GL104977, https://doi.org/10.1029/2023GL104977, 2023.

Cox, C. J., Walden, V. P., and Rowe, P. M.: A comparison of the atmospheric conditions at Eureka, Canada, and Barrow, Alaska (2006–2008), J. Geophys. Res. Atmospheres, 117, 2011JD017164, https://doi.org/10.1029/2011JD017164, 2012.

Cox, C. J., Walden, V. P., Rowe, P. M., and Shupe, M. D.: Humidity trends imply increased sensitivity to clouds in a warming Arctic, Nat. Commun., 6, 10117, https://doi.org/10.1038/ncomms10117, 2015.

https://doi.org/10.5194/egusphere-2025-2698
Preprint. Discussion started: 3 July 2025

Cronk et Partain: CloudSat ECMWF_AUX Auxillary Data Product Process Description and Interface Control Document, , 9th February, 15, 2017.

Curry, J. A. and Ebert, E. E.: Annual Cycle of Radiation Fluxes over the Arctic Ocean: Sensitivity to Cloud Optical Properties, J. Clim., 5, 1267–1280, https://doi.org/10.1175/1520-0442(1992)005<1267:ACORFO>2.0.CO;2, 1992.

Curry, J. A., Schramm, J. L., Rossow, W. B., and Randall, D.: Overview of Arctic Cloud and Radiation Characteristics, J. Clim., 9, 1731–1764, https://doi.org/10.1175/1520-0442(1996)009<1731:OOACAR>2.0.CO;2, 1996.

De Boer, G., Eloranta, E. W., and Shupe, M. D.: Arctic Mixed-Phase Stratiform Cloud Properties from Multiple Years of Surface-Based Measurements at Two High-Latitude Locations, J. Atmospheric Sci., 66, 2874–2887, https://doi.org/10.1175/2009JAS3029.1, 2009.

Delanoë, J. and Hogan, R. J.: A variational scheme for retrieving ice cloud properties from combined radar, lidar, and infrared radiometer, J. Geophys. Res. Atmospheres, 113, 2007JD009000, https://doi.org/10.1029/2007JD009000, 2008.

Delanoë, J. and Hogan, R. J.: Combined CloudSat-CALIPSO-MODIS retrievals of the properties of ice clouds, J. Geophys. Res., 115, D00H29, https://doi.org/10.1029/2009JD012346, 2010.

Delanoë, J., Hogan, R. J., Forbes, R. M., Bodas-Salcedo, A., and Stein, T. H. M.: Evaluation of ice cloud representation in the ECMWF and UK Met Office models using CloudSat and CALIPSO data, Q. J. R. Meteorol. Soc., 137, 2064–2078, https://doi.org/10.1002/qj.882, 2011.

Dong, X., Xi, B., Crosby, K., Long, C. N., Stone, R. S., and Shupe, M. D.: A 10 year climatology of Arctic cloud fraction and radiative forcing at Barrow, Alaska, J. Geophys. Res. Atmospheres, 115, 2009JD013489, https://doi.org/10.1029/2009JD013489, 2010.

Du, J., Kimball, J. S., Jones, L. A., Kim, Y., Glassy, J., and Watts, J. D.: A global satellite environmental data record derived from AMSR-E and AMSR2 microwave Earth observations, Earth Syst. Sci. Data, 9, 791–808, https://doi.org/10.5194/essd-9-791-2017, 2017.

Eastman, R. and Warren, S. G.: Interannual Variations of Arctic Cloud Types in Relation to Sea Ice, J. Clim., 23, 4216–4232, https://doi.org/10.1175/2010JCLI3492.1, 2010.

Ebell, K., Nomokonova, T., Maturilli, M., and Ritter, C.: Radiative Effect of Clouds at Ny-Ålesund, Svalbard, as Inferred from Ground-Based Remote Sensing Observations, J. Appl. Meteorol. Climatol., 59, 3–22, https://doi.org/10.1175/JAMC-D-19-0080.1, 2020.

Fletcher, J., Mason, S., and Jakob, C.: The Climatology, Meteorology, and Boundary Layer Structure of Marine Cold Air Outbreaks in Both Hemispheres*, J. Clim., 29, 1999–2014, https://doi.org/10.1175/JCLI-D-15-0268.1, 2016.

https://doi.org/10.5194/egusphere-2025-2698
Preprint. Discussion started: 3 July 2025

Gierens, R., Kneifel, S., Shupe, M. D., Ebell, K., Maturilli, M., and Löhnert, U.: Low-level mixed-phase clouds in a complex Arctic environment, Atmospheric Chem. Phys., 20, 3459–3481, https://doi.org/10.5194/acp-20-3459-2020, 2020.

Grace, J. B., Johnson, D. J., Lefcheck, J. S., and Byrnes, J. E. K.: Quantifying relative importance: computing standardized effects in models with binary outcomes, Ecosphere, 9, e02283, https://doi.org/10.1002/ecs2.2283, 2018.

Griesche, H. J., Ohneiser, K., Seifert, P., Radenz, M., Engelmann, R., and Ansmann, A.: Contrasting ice formation in Arctic clouds: surface-coupled vs. surface-decoupled clouds, Atmospheric Chem. Phys., 21, 10357–10374, https://doi.org/10.5194/acp-21-10357-2021, 2021.

Hersbach, H., Bell, B., Berrisford, P., Hirahara, S., Horányi, A., Muñoz-Sabater, J., Nicolas, J., Peubey, C., Radu, R., Schepers, D., Simmons, A., Soci, C., Abdalla, S., Abellan, X., Balsamo, G., Bechtold, P., Biavati, G., Bidlot, J., Bonavita, M., De Chiara, G., Dahlgren, P., Dee, D., Diamantakis, M., Dragani, R., Flemming, J., Forbes, R., Fuentes, M., Geer, A., Haimberger, L., Healy, S., Hogan, R. J., Hólm, E., Janisková, M., Keeley, S., Laloyaux, P., Lopez, P., Lupu, C., Radnoti, G., De Rosnay, P., Rozum, I., Vamborg, F., Villaume, S., and Thépaut, J.: The ERA5 global reanalysis, Q. J. R. Meteorol. Soc., 146, 1999–2049, https://doi.org/10.1002/qj.3803, 2020.

Inoue, J., Liu, J., Pinto, J. O., and Curry, J. A.: Intercomparison of Arctic Regional Climate Models: Modeling Clouds and Radiation for SHEBA in May 1998, J. Clim., 19, 4167–4178, https://doi.org/10.1175/JCLI3854.1, 2006.

Intrieri, J. M., Shupe, M. D., Uttal, T., and McCarty, B. J.: An annual cycle of Arctic cloud characteristics observed by radar and lidar at SHEBA, J. Geophys. Res. Oceans, 107, https://doi.org/10.1029/2000JC000423, 2002.

Järvinen, E., Nehlert, F., Xu, G., Waitz, F., Mioche, G., Dupuy, R., Jourdan, O., and Schnaiter, M.: Investigating the vertical extent and short-wave radiative effects of the ice phase in Arctic summertime low-level clouds, Atmospheric Chem. Phys., 23, 7611–7633, https://doi.org/10.5194/acp-23-7611-2023, 2023.

Jiang, Z., Ding, M., Zhong, L., Li, Y., and Hu, X.: Seasonal variations of Arctic cloud in recent 14 years using CALIPSO-GOCCP, Atmospheric Res., 309, 107598, https://doi.org/10.1016/j.atmosres.2024.107598, 2024.

Kay, J. E. and Gettelman, A.: Cloud influence on and response to seasonal Arctic sea ice loss, J. Geophys. Res. Atmospheres, 114, 2009JD011773, https://doi.org/10.1029/2009JD011773, 2009.

Kay, J. E. and L'Ecuyer, T.: Observational constraints on Arctic Ocean clouds and radiative fluxes during the early 21st century: ARCTIC OCEAN CLOUD AND RADIATION CLIMATOLOGY, J. Geophys. Res. Atmospheres, 118, 7219–7236, https://doi.org/10.1002/jgrd.50489, 2013.

Kay, J. E., L'Ecuyer, T., Chepfer, H., Loeb, N., Morrison, A., and Cesana, G.: Recent Advances in Arctic Cloud and Climate Research, Curr. Clim. Change Rep., 2, 159–169, https://doi.org/10.1007/s40641-016-0051-9, 2016.

Koike, M., Ukita, J., Ström, J., Tunved, P., Shiobara, M., Vitale, V., Lupi, A., Baumgardner, D., Ritter, C., Hermansen, O., Yamada, K., and Pedersen, C. A.: Year-Round In Situ Measurements of Arctic Low-Level

https://doi.org/10.5194/egusphere-2025-2698
Preprint. Discussion started: 3 July 2025

Clouds: Microphysical Properties and Their Relationships With Aerosols, J. Geophys. Res. Atmospheres, 124, 1798–1822, https://doi.org/10.1029/2018JD029802, 2019.

Kotarba, A. Z. and Solecki, M.: Uncertainty Assessment of the Vertically-Resolved Cloud Amount for Joint CloudSat–CALIPSO Radar–Lidar Observations, Remote Sens., 13, 807, https://doi.org/10.3390/rs13040807, 2021.

Lackner, C. P., Geerts, B., Juliano, T. W., Xue, L., and Kosovic, B.: Vertical Structure of Clouds and Precipitation During Arctic Cold-Air Outbreaks and Warm-Air Intrusions: Observations From COMBLE, J. Geophys. Res. Atmospheres, 128, e2022JD038403, https://doi.org/10.1029/2022JD038403, 2023.

Law, K. S., Stohl, A., Quinn, P. K., Brock, C. A., Burkhart, J. F., Paris, J.-D., Ancellet, G., Singh, H. B., Roiger, A., Schlager, H., Dibb, J., Jacob, D. J., Arnold, S. R., Pelon, J., and Thomas, J. L.: Arctic Air Pollution: New Insights from POLARCAT-IPY, Bull. Am. Meteorol. Soc., 95, 1873–1895, https://doi.org/10.1175/BAMS-D-13-00017.1, 2014.

Legendre, P. and Legendre, L.: Numerical ecology, Third English edition., Elsevier, Amsterdam, 990 pp., 2012.

Lelli, L., Vountas, M., Khosravi, N., and Burrows, J. P.: Satellite remote sensing of regional and seasonal Arctic cooling showing a multi-decadal trend towards brighter and more liquid clouds, Atmospheric Chem. Phys., 23, 2579–2611, https://doi.org/10.5194/acp-23-2579-2023, 2023.

Li, X., Krueger, S. K., Strong, C., Mace, G. G., and Benson, S.: Midwinter Arctic leads form and dissipate low clouds, Nat. Commun., 11, 206, https://doi.org/10.1038/s41467-019-14074-5, 2020a.

Li, X., Krueger, S. K., Strong, C., and Mace, G. G.: Relationship Between Wintertime Leads and Low Clouds in the Pan-Arctic, J. Geophys. Res. Atmospheres, 125, e2020JD032595, https://doi.org/10.1029/2020JD032595, 2020b.

Li, X., Mace, G. G., Strong, C., and Krueger, S. K.: Wintertime Cooling of the Arctic TOA by Low-Level Clouds, Geophys. Res. Lett., 50, e2023GL104869, https://doi.org/10.1029/2023GL104869, 2023.

Listowski, C., Delanoë, J., Kirchgaessner, A., Lachlan-Cope, T., and King, J.: Antarctic clouds, supercooled liquid water and mixed phase, investigated with DARDAR: geographical and seasonal variations, Atmospheric Chem. Phys., 19, 6771–6808, https://doi.org/10.5194/acp-19-6771-2019, 2019.

Liu, X., He, T., Liang, S., Li, R., Xiao, X., Ma, R., and Ma, Y.: A monthly 1° resolution dataset of daytime cloud fraction over the Arctic during 2000–2020 based on multiple satellite products, Earth Syst. Sci. Data, 15, 3641–3671, https://doi.org/10.5194/essd-15-3641-2023, 2023.

Liu, Y.: Impacts of active satellite sensors' low-level cloud detection limitations on cloud radiative forcing in the Arctic, Atmospheric Chem. Phys., 22, 8151–8173, https://doi.org/10.5194/acp-22-8151-2022, 2022.

Liu, Y., Heuvelink, G. B. M., Bai, Z., He, P., Xu, X., Ding, W., and Huang, S.: Analysis of spatio-temporal variation of crop yield in China using stepwise multiple linear regression, Field Crops Res., 264, 108098, https://doi.org/10.1016/j.fcr.2021.108098, 2021.

https://doi.org/10.5194/egusphere-2025-2698
Preprint. Discussion started: 3 July 2025

Liu, Z. and Schweiger, A.: Synoptic Conditions, Clouds, and Sea Ice Melt Onset in the Beaufort and Chukchi Seasonal Ice Zone, J. Clim., 30, 6999–7016, https://doi.org/10.1175/JCLI-D-16-0887.1, 2017.

Liu, Z. and Schweiger, A.: ICESat-2 Shows Sea Ice Leads Have Little Overall Effects on the Arctic Cloudiness in Cold Months, J. Clim., 37, 4045–4058, https://doi.org/10.1175/JCLI-D-23-0285.1, 2024.

Liu, Z., Vaughan, M., Winker, D., Kittaka, C., Getzewich, B., Kuehn, R., Omar, A., Powell, K., Trepte, C., and Hostetler, C.: The CALIPSO Lidar Cloud and Aerosol Discrimination: Version 2 Algorithm and Initial Assessment of Performance, J. Atmospheric Ocean. Technol., 26, 1198–1213, https://doi.org/10.1175/2009JTECHA1229.1, 2009.

Liu, Z., Kar, J., Zeng, S., Tackett, J., Vaughan, M., Avery, M., Pelon, J., Getzewich, B., Lee, K.-P., Magill, B., Omar, A., Lucker, P., Trepte, C., and Winker, D.: Discriminating between clouds and aerosols in the CALIOP version 4.1 data products, Atmospheric Meas. Tech., 12, 703–734, https://doi.org/10.5194/amt-12-703-2019, 2019.

Marchand, R., Mace, G. G., Ackerman, T., and Stephens, G.: Hydrometeor Detection Using Cloudsat—An Earth-Orbiting 94-GHz Cloud Radar, J. Atmospheric Ocean. Technol., 25, 519–533, https://doi.org/10.1175/2007JTECHA1006.1, 2008.

Matus, A. V. and L'Ecuyer, T. S.: The role of cloud phase in Earth's radiation budget, J. Geophys. Res. Atmospheres, 122, 2559–2578, https://doi.org/10.1002/2016JD025951, 2017.

McFarquhar, G. M., Zhang, G., Poellot, M. R., Kok, G. L., McCoy, R., Tooman, T., Fridlind, A., and Heymsfield, A. J.: Ice properties of single-layer stratocumulus during the Mixed-Phase Arctic Cloud Experiment: 1. Observations, J. Geophys. Res. Atmospheres, 112, 2007JD008633, https://doi.org/10.1029/2007JD008633, 2007.

McGill, M. J., Vaughan, M. A., Trepte, C. R., Hart, W. D., Hlavka, D. L., Winker, D. M., and Kuehn, R.: Airborne validation of spatial properties measured by the CALIPSO lidar, J. Geophys. Res. Atmospheres, 112, 2007JD008768, https://doi.org/10.1029/2007JD008768, 2007.

McIlhattan, E. A., L'Ecuyer, T. S., and Miller, N. B.: Observational Evidence Linking Arctic Supercooled Liquid Cloud Biases in CESM to Snowfall Processes, J. Clim., 30, 4477–4495, https://doi.org/10.1175/JCLI-D-16-0666.1, 2017.

Michaelis, J., Schmitt, A. U., Lüpkes, C., Hartmann, J., Birnbaum, G., and Vihma, T.: Observations of marine cold-air outbreaks: a comprehensive data set of airborne and dropsonde measurements from the Springtime Atmospheric Boundary Layer Experiment (STABLE), Earth Syst. Sci. Data, 14, 1621–1637, https://doi.org/10.5194/essd-14-1621-2022, 2022.

Miller, N. B., Shupe, M. D., Cox, C. J., Walden, V. P., Turner, D. D., and Steffen, K.: Cloud Radiative Forcing at Summit, Greenland, J. Clim., 28, 6267–6280, https://doi.org/10.1175/JCLI-D-15-0076.1, 2015.

Mioche, G. and Jourdan, O.: Spaceborne Remote Sensing and Airborne In Situ Observations of Arctic Mixed-Phase Clouds, in: Mixed-Phase Clouds, Elsevier, 121–150, https://doi.org/10.1016/B978-0-12-810549-8.00006-4, 2018.

https://doi.org/10.5194/egusphere-2025-2698
Preprint. Discussion started: 3 July 2025

Mioche, G., Jourdan, O., Ceccaldi, M., and Delanoë, J.: Variability of mixed-phase clouds in the Arctic with a focus on the Svalbard region: a study based on spaceborne active remote sensing, Atmospheric Chem. Phys., 15, 2445–2461, https://doi.org/10.5194/acp-15-2445-2015, 2015.

Mioche, G., Jourdan, O., Delanoë, J., Gourbeyre, C., Febvre, G., Dupuy, R., Monier, M., Szczap, F., Schwarzenboeck, A., and Gayet, J.-F.: Vertical distribution of microphysical properties of Arctic springtime low-level mixed-phase clouds over the Greenland and Norwegian seas, Atmospheric Chem. Phys., 17, 12845–12869, https://doi.org/10.5194/acp-17-12845-2017, 2017.

Morrison, A. L., Kay, J. E., Chepfer, H., Guzman, R., and Yettella, V.: Isolating the Liquid Cloud Response to Recent Arctic Sea Ice Variability Using Spaceborne Lidar Observations, J. Geophys. Res. Atmospheres, 123, 473–490, https://doi.org/10.1002/2017JD027248, 2018.

Morrison, A. L., Kay, J. E., Frey, W. R., Chepfer, H., and Guzman, R.: Cloud Response to Arctic Sea Ice Loss and Implications for Future Feedback in the CESM1 Climate Model, J. Geophys. Res. Atmospheres, 124, 1003–1020, https://doi.org/10.1029/2018JD029142, 2019.

Morrison, H., De Boer, G., Feingold, G., Harrington, J., Shupe, M. D., and Sulia, K.: Resilience of persistent Arctic mixed-phase clouds, Nat. Geosci., 5, 11–17, https://doi.org/10.1038/ngeo1332, 2012.

Moser, M., Voigt, C., Jurkat-Witschas, T., Hahn, V., Mioche, G., Jourdan, O., Dupuy, R., Gourbeyre, C., Schwarzenboeck, A., Lucke, J., Boose, Y., Mech, M., Borrmann, S., Ehrlich, A., Herber, A., Lüpkes, C., and Wendisch, M.: Microphysical and thermodynamic phase analyses of Arctic low-level clouds measured above the sea ice and the open ocean in spring and summer, Atmospheric Chem. Phys., 23, 7257–7280, https://doi.org/10.5194/acp-23-7257-2023, 2023.

Murray-Watson, R. J., Gryspeerdt, E., and Goren, T.: Investigating the development of clouds within marine cold-air outbreaks, Atmospheric Chem. Phys., 23, 9365–9383, https://doi.org/10.5194/acp-23-9365-2023, 2023.

Narizhnaya, A. and Chernokulsky, A.: Cloud Characteristics during Intense Cold Air Outbreaks over the Barents Sea Based on Satellite Data, Atmosphere, 15, 317, https://doi.org/10.3390/atmos15030317, 2024.

Naud, C. M., Elsaesser, G. S., and Booth, J. F.: Dominant Cloud Controlling Factors for Low-Level Cloud Fraction: Subtropical Versus Extratropical Oceans, Geophys. Res. Lett., 50, e2023GL104496, https://doi.org/10.1029/2023GL104496, 2023.

Noel, V., Chepfer, H., Chiriaco, M., and Yorks, J.: The diurnal cycle of cloud profiles over land and ocean between 51° S and 51° N, seen by the CATS spaceborne lidar from the International Space Station, Atmospheric Chem. Phys., 18, 9457–9473, https://doi.org/10.5194/acp-18-9457-2018, 2018.

Nomokonova, T., Ebell, K., Löhnert, U., Maturilli, M., Ritter, C., and O'Connor, E.: Statistics on clouds and their relation to thermodynamic conditions at Ny-Ålesund using ground-based sensor synergy, Atmospheric Chem. Phys., 19, 4105–4126, https://doi.org/10.5194/acp-19-4105-2019, 2019.

https://doi.org/10.5194/egusphere-2025-2698
Preprint. Discussion started: 3 July 2025

Philipp, D., Stengel, M., and Ahrens, B.: Analyzing the Arctic Feedback Mechanism between Sea Ice and Low-Level Clouds Using 34 Years of Satellite Observations, J. Clim., 33, 7479–7501, https://doi.org/10.1175/JCLI-D-19-0895.1, 2020.

Rangno, A. L. and Hobbs, P. V.: Ice particles in stratiform clouds in the Arctic and possible mechanisms for the production of high ice concentrations, J. Geophys. Res. Atmospheres, 106, 15065–15075, https://doi.org/10.1029/2000JD900286, 2001.

Rantanen, M., Karpechko, A. Yu., Lipponen, A., Nordling, K., Hyvärinen, O., Ruosteenoja, K., Vihma, T., and Laaksonen, A.: The Arctic has warmed nearly four times faster than the globe since 1979, Commun. Earth Environ., 3, 168, https://doi.org/10.1038/s43247-022-00498-3, 2022.

Raschke, E., Kinne, S., Rossow, W. B., Stackhouse, P. W., and Wild, M.: Comparison of Radiative Energy Flows in Observational Datasets and Climate Modeling, J. Appl. Meteorol. Climatol., 55, 93–117, https://doi.org/10.1175/JAMC-D-14-0281.1, 2016.

Raut, J.-C., Law, K. S., Onishi, T., Daskalakis, N., and Marelle, L.: Impact of shipping emissions on air pollution and pollutant deposition over the Barents Sea, Environ. Pollut., 298, 118832, https://doi.org/10.1016/j.envpol.2022.118832, 2022.

Schmale, J., Zieger, P., and Ekman, A. M. L.: Aerosols in current and future Arctic climate, Nat. Clim. Change, 11, 95–105, https://doi.org/10.1038/s41558-020-00969-5, 2021.

Schweiger, A. J. and Key, J. R.: Arctic Cloudiness. Comparison of ISCCP-C2 and *Nimbus-7* Satellite-derived Cloud Products with a Surface-based Cloud Climatology, J. Clim., 5, 1514–1527, https://doi.org/10.1175/1520-0442(1992)005<1514:ACCOIC>2.0.CO;2, 1992.

Scott, R. C., Myers, T. A., Norris, J. R., Zelinka, M. D., Klein, S. A., Sun, M., and Doelling, D. R.: Observed Sensitivity of Low-Cloud Radiative Effects to Meteorological Perturbations over the Global Oceans, J. Clim., 33, 7717–7734, https://doi.org/10.1175/JCLI-D-19-1028.1, 2020.

Screen, J. A. and Simmonds, I.: Increasing fall-winter energy loss from the Arctic Ocean and its role in Arctic temperature amplification, Geophys. Res. Lett., 37, 2010GL044136, https://doi.org/10.1029/2010GL044136, 2010.

Sedlar, J., Shupe, M. D., and Tjernström, M.: On the Relationship between Thermodynamic Structure and Cloud Top, and Its Climate Significance in the Arctic, J. Clim., 25, 2374–2393, https://doi.org/10.1175/JCLI-D-11-00186.1, 2012.

Sharafi, S. and Ghaleni, M. M.: Evaluation of multivariate linear regression for reference evapotranspiration modeling in different climates of Iran, Theor. Appl. Climatol., 143, 1409–1423, https://doi.org/10.1007/s00704-020-03473-0, 2021.

Shibata, A., Imaoka, K., and Koike, T.: AMSR/AMSR-E level 2 and 3 algorithm developments and data validation plans of NASDA, IEEE Trans. Geosci. Remote Sens., 41, 195–203, https://doi.org/10.1109/TGRS.2002.808320, 2003.

https://doi.org/10.5194/egusphere-2025-2698
Preprint. Discussion started: 3 July 2025

Shupe, M. D. and Intrieri, J. M.: Cloud Radiative Forcing of the Arctic Surface: The Influence of Cloud Properties, Surface Albedo, and Solar Zenith Angle, J. Clim., 17, 616–628, https://doi.org/10.1175/1520-0442(2004)017<0616:CRFOTA>2.0.CO;2, 2004.

Shupe, M. D., Matrosov, S. Y., and Uttal, T.: Arctic Mixed-Phase Cloud Properties Derived from Surface-Based Sensors at SHEBA, J. Atmospheric Sci., 63, 697–711, https://doi.org/10.1175/JAS3659.1, 2006.

Shupe, M. D., Walden, V. P., Eloranta, E., Uttal, T., Campbell, J. R., Starkweather, S. M., and Shiobara, M.: Clouds at Arctic Atmospheric Observatories. Part I: Occurrence and Macrophysical Properties, J. Appl. Meteorol. Climatol., 50, 626–644, https://doi.org/10.1175/2010JAMC2467.1, 2011.

Spreen, G., Kaleschke, L., and Heygster, G.: Sea ice remote sensing using AMSR-E 89-GHz channels, J. Geophys. Res. Oceans, 113, 2005JC003384, https://doi.org/10.1029/2005JC003384, 2008.

Stephens, G. L., Vane, D. G., Boain, R. J., Mace, G. G., Sassen, K., Wang, Z., Illingworth, A. J., O'connor, E. J., Rossow, W. B., Durden, S. L., Miller, S. D., Austin, R. T., Benedetti, A., Mitrescu, C., and the CloudSat Science Team: THE CLOUDSAT MISSION AND THE A-TRAIN: A New Dimension of Space-Based Observations of Clouds and Precipitation, Bull. Am. Meteorol. Soc., 83, 1771–1790, https://doi.org/10.1175/BAMS-83-12-1771, 2002.

Stroeve, J. C., Serreze, M. C., Holland, M. M., Kay, J. E., Malanik, J., and Barrett, A. P.: The Arctic's rapidly shrinking sea ice cover: a research synthesis, Clim. Change, 110, 1005–1027, https://doi.org/10.1007/s10584-011-0101-1, 2012.

Sun, Z. and Shine, K. P.: Studies of the radiative properties of ice and mixed-phase clouds, Q. J. R. Meteorol. Soc., 120, 111–137, https://doi.org/10.1002/qj.49712051508, 1994.

Tan, I., Sotiropoulou, G., Taylor, P. C., Zamora, L., and Wendisch, M.: A Review of the Factors Influencing Arctic Mixed-Phase Clouds: Progress and Outlook, in: Geophysical Monograph Series, edited by: Sullivan, S. C. and Hoose, C., Wiley, 103–132, https://doi.org/10.1002/9781119700357.ch5, 2023.

Taylor, P. C. and Monroe, E.: Isolating the Surface Type Influence on Arctic Low-Clouds, J. Geophys. Res. Atmospheres, 128, e2022JD038098, https://doi.org/10.1029/2022JD038098, 2023.

Taylor, P. C., Boeke, R. C., Li, Y., and Thompson, D. W. J.: Arctic cloud annual cycle biases in climate models, Atmospheric Chem. Phys., 19, 8759–8782, https://doi.org/10.5194/acp-19-8759-2019, 2019.

Tjernström, M., Sedlar, J., and Shupe, M. D.: How Well Do Regional Climate Models Reproduce Radiation and Clouds in the Arctic? An Evaluation of ARCMIP Simulations, J. Appl. Meteorol. Climatol., 47, 2405–2422, https://doi.org/10.1175/2008JAMC1845.1, 2008.

Vavrus, S., Waliser, D., Schweiger, A., and Francis, J.: Simulations of 20th and 21st century Arctic cloud amount in the global climate models assessed in the IPCC AR4, Clim. Dyn., 33, 1099–1115, https://doi.org/10.1007/s00382-008-0475-6, 2009.

https://doi.org/10.5194/egusphere-2025-2698
Preprint. Discussion started: 3 July 2025

Wang, X. and Key, J. R.: Arctic Surface, Cloud, and Radiation Properties Based on the AVHRR Polar Pathfinder Dataset. Part I: Spatial and Temporal Characteristics, J. Clim., 18, 2558–2574, https://doi.org/10.1175/JCLI3438.1, 2005.

Wang, X., Liu, J., Yang, B., Bao, Y., Petropoulos, G. P., Liu, H., and Hu, B.: Seasonal Trends in Clouds and Radiation over the Arctic Seas from Satellite Observations during 1982 to 2019, Remote Sens., 13, 3201, https://doi.org/10.3390/rs13163201, 2021.

Wendisch, M., Macke, A., Ehrlich, A., Lüpkes, C., Mech, M., Chechin, D., Dethloff, K., Velasco, C. B., Bozem, H., Brückner, M., Clemen, H.-C., Crewell, S., Donth, T., Dupuy, R., Ebell, K., Egerer, U., Engelmann, R., Engler, C., Eppers, O., Gehrmann, M., Gong, X., Gottschalk, M., Gourbeyre, C., Griesche, H., Hartmann, J., Hartmann, M., Heinold, B., Herber, A., Herrmann, H., Heygster, G., Hoor, P., Jafariserajehlou, S., Jäkel, E., Järvinen, E., Jourdan, O., Kästner, U., Kecorius, S., Knudsen, E. M., Köllner, F., Kretzschmar, J., Lelli, L., Leroy, D., Maturilli, M., Mei, L., Mertes, S., Mioche, G., Neuber, R., Nicolaus, M., Nomokonova, T., Notholt, J., Palm, M., Van Pinxteren, M., Quaas, J., Richter, P., Ruiz-Donoso, E., Schäfer, M., Schmieder, K., Schnaiter, M., Schneider, J., Schwarzenböck, A., Seifert, P., Shupe, M. D., Siebert, H., Spreen, G., Stapf, J., Stratmann, F., Vogl, T., Welti, A., Wex, H., Wiedensohler, A., Zanatta, M., and Zeppenfeld, S.: The Arctic Cloud Puzzle: Using ACLOUD/PASCAL Multiplatform Observations to Unravel the Role of Clouds and Aerosol Particles in Arctic Amplification, Bull. Am. Meteorol. Soc., 100, 841–871, https://doi.org/10.1175/BAMS-D-18-0072.1, 2019.

Wiebe, H., Heygster, G., and Markus, T.: Comparison of the ASI Ice Concentration Algorithm With Landsat-7 ETM+ and SAR Imagery, IEEE Trans. Geosci. Remote Sens., 47, 3008–3015, https://doi.org/10.1109/TGRS.2009.2026367, 2009.

Willis, M. D., Bozem, H., Kunkel, D., Lee, A. K. Y., Schulz, H., Burkart, J., Aliabadi, A. A., Herber, A. B., Leaitch, W. R., and Abbatt, J. P. D.: Aircraft-based measurements of High Arctic springtime aerosol show evidence for vertically varying sources, transport and composition, Atmospheric Chem. Phys., 19, 57–76, https://doi.org/10.5194/acp-19-57-2019, 2019.

Winker, D. M., Hunt, W. H., and McGill, M. J.: Initial performance assessment of CALIOP, Geophys. Res. Lett., 34, 2007GL030135, https://doi.org/10.1029/2007GL030135, 2007.

Wood, R. and Bretherton, C. S.: On the Relationship between Stratiform Low Cloud Cover and Lower-Tropospheric Stability, J. Clim., 19, 6425–6432, https://doi.org/10.1175/JCLI3988.1, 2006.

Woods, C. and Caballero, R.: The Role of Moist Intrusions in Winter Arctic Warming and Sea Ice Decline, J. Clim., 29, 4473–4485, https://doi.org/10.1175/JCLI-D-15-0773.1, 2016.

Wu, P. and Ovchinnikov, M.: Cloud Morphology Evolution in Arctic Cold-Air Outbreak: Two Cases During COMBLE Period, J. Geophys. Res. Atmospheres, 127, e2021JD035966, https://doi.org/10.1029/2021JD035966, 2022.

Wyser, K., Jones, C. G., Du, P., Girard, E., Willén, U., Cassano, J., Christensen, J. H., Curry, J. A., Dethloff, K., Haugen, J.-E., Jacob, D., Køltzow, M., Laprise, R., Lynch, A., Pfeifer, S., Rinke, A., Serreze, M., Shaw, M. J., Tjernström, M., and Zagar, M.: An evaluation of Arctic cloud and radiation processes during the SHEBA year:

https://doi.org/10.5194/egusphere-2025-2698
Preprint. Discussion started: 3 July 2025

simulation results from eight Arctic regional climate models, Clim. Dyn., 30, 203–223, https://doi.org/10.1007/s00382-007-0286-1, 2008.

Yan, Y., Liu, X., Liu, Y., and Lu, J.: Comparison of mixed-phase clouds over the Arctic and the Tibetan Plateau: seasonality and vertical structure of cloud radiative effects, Clim. Dyn., 54, 4811–4822, https://doi.org/10.1007/s00382-020-05257-8, 2020.

Young, G., Connolly, P. J., Dearden, C., and Choularton, T. W.: Relating large-scale subsidence to convection development in Arctic mixed-phase marine stratocumulus, Atmospheric Chem. Phys., 18, 1475–1494, https://doi.org/10.5194/acp-18-1475-2018, 2018.

Young, S. A. and Vaughan, M. A.: The Retrieval of Profiles of Particulate Extinction from Cloud-Aerosol Lidar Infrared Pathfinder Satellite Observations (CALIPSO) Data: Algorithm Description, J. Atmospheric Ocean. Technol., 26, 1105–1119, https://doi.org/10.1175/2008JTECHA1221.1, 2009.

Yu, Y., Taylor, P. C., and Cai, M.: Seasonal Variations of Arctic Low-Level Clouds and Its Linkage to Sea Ice Seasonal Variations, J. Geophys. Res. Atmospheres, 124, 12206–12226, https://doi.org/10.1029/2019JD031014, 2019.

Zanatta, M., Mertes, S., Jourdan, O., Dupuy, R., Järvinen, E., Schnaiter, M., Eppers, O., Schneider, J., Jurányi, Z., and Herber, A.: Airborne investigation of black carbon interaction with low-level, persistent, mixed-phase clouds in the Arctic summer, Atmospheric Chem. Phys., 23, 7955–7973, https://doi.org/10.5194/acp-23-7955-2023, 2023.

Zhang, X., Tang, H., Zhang, J., Walsh, J. E., Roesler, E. L., Hillman, B., Ballinger, T. J., and Weijer, W.: Arctic cyclones have become more intense and longer-lived over the past seven decades, Commun. Earth Environ., 4, 348, https://doi.org/10.1038/s43247-023-01003-0, 2023.